

Improving Geologic and Engineering Models of Midcontinent Fracture and Karst-Modified Reservoirs Using New 3-D Seismic Attributes

Type of Report: Semiannual Scientific/Technical

Reporting Period Start Date: October 1, 2005

Reporting Period End Date: March 31, 2006

Principal Authors:

Susan E. Nissen, Kansas Geological Survey, University of Kansas, Lawrence, Kansas
Natalie B. Givens, Kansas Geological Survey, University of Kansas, Lawrence, Kansas
John H. Doveton, Kansas Geological Survey, University of Kansas, Lawrence, Kansas
Alan P. Byrnes, Kansas Geological Survey, University of Kansas, Lawrence, Kansas
Benjamin J. Rocke, Kansas Geological Survey, University of Kansas, Lawrence, Kansas
Saibal Bhattacharya, Kansas Geological Survey, University of Kansas, Lawrence, Kansas
E. Charlotte Sullivan, Pacific Northwest National Labs, Richland, Washington

Date Report was Issued: May 2006

DOE Award Number: DE-FC26-04NT15504

Submitting Organizations:

The University of Kansas Center for Research, Inc
2385 Irving Hill Road
Lawrence, Kansas 66045-7563

Allied Geophysical Laboratories
Department of Geosciences
University of Houston
Houston, Texas 77204-5505

DISCLAIMER

This report was prepared as an account of work sponsored by an agency of the United States Government. Neither the United States Government nor any agency thereof, nor any of their employees, makes any warranty, express or implied, or assumes any legal liability or responsibility for the accuracy, completeness, or usefulness of any information, apparatus, product, or process disclosed, or represents that its use would not infringe privately owned rights. Reference herein to any specific commercial product, process, or service by trade name, trademark, manufacturer, or otherwise does not necessarily constitute or imply its endorsement, recommendation, or favoring by the United States Government or any agency thereof. The views and opinions of authors expressed herein do not necessarily state or reflect those of the United States Government or any agency thereof.

ABSTRACT

We are conducting an integrated study, including reservoir characterization, geomodel building, and reservoir simulation, of three Midcontinent karst-modified reservoirs: the Permian San Andres in west Texas, the Mississippian Spergen in Colorado, and the Ordovician Arbuckle in Kansas, in order to address our project goal of developing innovative seismic-based workflows for the incremental recovery of oil from karst-modified reservoirs within the onshore continental United States.

During this third reporting period, from October 1, 2005, through March 31, 2006, we have made significant progress in reservoir characterization for our three study areas and have developed a workflow for geomodel building. Our primary focus for the San Andres and Mississippian study areas has been to estimate key petrophysical parameters from core and log data and make seismically-based interpretations of reservoir compartment boundaries and vertical fluid conduits for input into reservoir geomodels. For the Arbuckle study area, we have characterized karst geomorphology on a regional scale, since different terrains exhibit differences in oil productivity. We have also used geostatistical analyses of the 3-D seismic data to predict the probability of untapped remnant Arbuckle highs between existing wells in areas where there is no seismic data.

Technology transfer activities included presentations of project results at regional and national conferences, as well as posting of information related to the project (including project background, personnel, a catalog of seismic karst features, publications, and semi-annual scientific/technical reports) on our project website:

<http://www.kgs.ku.edu/SEISKARST>.

TABLE OF CONTENTS

TITLE PAGE 1

DISCLAIMER 2

ABSTRACT 3

TABLE OF CONTENTS 4

EXECUTIVE SUMMARY 5

1.0 INTRODUCTION 7

2.0 RESERVOIR CHARACTERIZATION STUDIES 8

 2.1 Permian San Andres Study Area 8

 2.2 Mississippian Study area 11

 2.3 Arbuckle Study Area 18

3.0 GEOMODEL CONSTRUCTION 20

4.0 TECHNOLOGY TRANSFER 21

5.0 CONCLUSIONS 22

LIST OF TABLES 24

LIST OF FIGURES 24

REFERENCES 28

TABLES 30

FIGURES 31

EXECUTIVE SUMMARY

We are conducting an integrated study of three karst-modified reservoirs: the Permian San Andres in west Texas, the Mississippian Spergen in Colorado, and the Ordovician Arbuckle in Kansas in order to (1) calibrate new multi-trace seismic attributes for improved imaging of karst-modified reservoirs, (2) develop attribute-based, cost-effective workflows to better characterize karst-modified carbonate reservoirs and fracture systems, and (3) improve accuracy and predictiveness of resulting geomodels and reservoir simulations. Our overall goal is to develop innovative seismic-based workflows for the incremental recovery of oil from karst-modified reservoirs within the onshore continental United States. During this third reporting period, from October 1, 2005, through March 31, 2006, the project was scheduled to focus on the following tasks: (1) complete reservoir characterization studies; (2) work on construction of integrated 3-D reservoir geomodels; (3) begin reservoir simulations; and 4) technology transfer. However, personnel changes have delayed progress on the project by approximately 4-6 months. In particular, geomodels are not yet constructed and reservoir simulation has not yet begun. Nonetheless, we have made significant progress in the reservoir characterization studies for all three study areas. Also, we have developed a workflow for geomodel building, identified gross reservoir layers, and obtained key petrophysical input parameters to the geomodel for the San Andres and Mississippian study areas.

Permian San Andres Study Area. The focus of the San Andres study during this reporting period has been to identify seismic attributes that have apparent correlation with compartment boundaries and fluid conduits and to develop petrophysical inputs for the geomodel. While there is no visual correlation between attributes plotted for the San Andres stratal surface and engineering-based interpretations of compartment boundaries, the Most Positive volumetric curvature extracted along a horizon approximately 500-600 ms below the San Andres reservoir shows lineaments that appear to truncate at the compartment boundaries in the overlying San Andres. We hypothesize that the lineament trends seen on this deeper surface relate to tectonic fractures that controlled preferred dissolution of anhydrite cement in the San Andres reservoir, connecting the reservoir with the underlying aquifer. Porosity and permeability inputs to the geomodel for the San Andres study area will be generated from predictive transforms applied to wireline logs that are calibrated with respect to core measurements. Log calibration was accomplished using a well in the study area containing 90 ft (27 m) of core with porosity and permeability data, as well as a full suite of neutron, density, and sonic porosity logs. A compositional model using neutron, density, and photoelectric logs that accommodates gypsum and anhydrite was found to be a good predictor of total porosity. Inclusion of the sonic log allowed partition of the pore space between interparticle porosity and coarser porosity, either as vugs within the karst zone or oomoldic porosity in an oolite shoal development. Predictive equations for porosity and permeability developed within this well will be applied in other wells that lack core and vary in their suite of wireline logs.

Mississippian Spergen Study Area. Reservoir characterization of the Spergen reservoir in the Mississippian study area is nearing completion and we have begun defining

parameters for input into the geomodel. We have constructed structure and isopach maps from key formation tops, and have divided the Spergen reservoir into three intervals, based on log response. Core description and thin section analysis for the two cores in the study area have allowed us to develop a hypothesized paragenesis for the Spergen. Core petrophysical analysis revealed a permeability-porosity relationship based on lithofacies. We have correlated petrophysical log properties to core data to allow for better prediction of petrophysical properties in non-cored wells. Pickett crossplots were used to analyze patterns in porosity, resistivity, and saturation in the reservoir, and to identify net pay. We have crossplotted average acoustic impedance for the Spergen interval extracted from a seismic inversion volume against porosities obtained from well logs, and found that, despite considerable scatter, there is a trend indicating that higher acoustic impedance corresponds to lower porosity. Well performance in the study area is extremely variable. Based on calculations from matrix porosities alone, some wells have performed better than expected, while others have under-performed. We have extracted Most Negative and Most Positive volumetric curvature along key horizons above and below the Spergen. Interpreted curvature lineaments show orientations that parallel regional structural orientations. The curvature lineaments may reflect subtle structural features, fractures or reservoir compartment boundaries that are the cause of the production inconsistencies.

Arbuckle Study Area. Arbuckle production is located on local remnant highs; however, not all wells drilled on the Arbuckle highs are productive. Reservoir characterization focuses on distinguishing tight Arbuckle from porous Arbuckle, as well as identifying the locations of the local structural highs. We have conducted a regional characterization of the Arbuckle erosional surface for an 1800 mi² (4662 km²) area centered on the seismic study area in order to characterize the regional karst geomorphology, as differences in oil productivity can be recognized between terrains. The Arbuckle surface in this area appears to be dominated by groundwater-sapped plateaus, half-blind valleys, and polygonal karst. Areas of highest Arbuckle production appear to be along up-tilted edges of blocks, where grainier horizons were preserved from groundwater-sapping processes. In the seismic study area, geomorphologies are reminiscent of polygonal karst, and the 3-D seismic map shows much more roughness in the surface of the Arbuckle than a map constructed from well tops alone. Geostatistical analyses making use of the 3-D seismic data are employed to predict roughness of the karst surface in areas where there is no seismic data. This method can be used to high-grade areas of potentially bypassed production trapped in local topographic closures.

Although we have not yet constructed geomodels for the study areas, we have developed a workflow for geomodel building, including a methodology for determining the parameters necessary for populating the geomodels. Several of these parameters have already been obtained for the Permian San Andres and the Mississippian Spergen reservoirs.

Technology transfer of our project work is being accomplished through presentations at professional society meetings and in associated publications, in Kansas Geological Survey Open-file reports, and in postings on the Kansas Geological Survey and University of Houston web sites.

1.0 INTRODUCTION

We are conducting an integrated study of three karst-modified reservoirs: the Permian San Andres in west Texas, the Mississippian Spergen in Colorado, and the Ordovician Arbuckle in Kansas (Figure 1.1) in order to (1) calibrate new multi-trace seismic attributes for improved imaging of karst-modified reservoirs, (2) develop attribute-based, cost-effective workflows to better characterize karst-modified carbonate reservoirs and fracture systems, and (3) improve accuracy and predictiveness of resulting geomodels and reservoir simulations. Our overall goal is to develop innovative seismic-based workflows for the incremental recovery of oil from karst-modified reservoirs within the onshore continental United States.

In the first two reporting periods, from October 1, 2004, through September 30, 2005, we (1) gathered 3-D seismic, petrophysical, and engineering data for all of our study areas, (2) generated multi-trace seismic attribute volumes (including coherence and volumetric curvature attributes) for the 3-D seismic surveys in all of our study areas, (3) generated a preliminary seismic attribute catalog of karst features (available online at <http://www.kgs.ku.edu/SEISKARST/catalog.html>); (4) began reservoir characterization studies (seismic, geological, petrophysical, and engineering) for all study areas; and 5) provided technology transfer through presentations at professional society meetings and postings to our project website (<http://www.kgs.ku.edu/SEISKARST>).

During this third reporting period, from October 1, 2005, through March 31, 2006, the project was scheduled to focus on the following tasks: (1) complete reservoir characterization studies; (2) work on construction of integrated 3-D reservoir geomodels; (3) begin reservoir simulations; and 4) technology transfer (Table 1.1). The reservoir characterization and geomodel construction for the Permian San Andres study area were originally to be conducted entirely at the University of Houston. However, in December 2005, University of Houston Project Manager Charlotte Sullivan left the University of Houston to take a position at the Pacific Northwest National Labs, and much of the San Andres geological and petrophysical work, as well as the geomodel construction, was transferred to the Kansas Geological Survey. Because of the change in personnel working on this study area, progress on the project is behind schedule by approximately 4-6 months. In particular, geomodels have not yet been constructed for each of the study areas and reservoir simulation has not yet begun. Nonetheless, significant progress has been made in the reservoir characterization studies for all three study areas. Also, a workflow for geomodel building has been developed, gross reservoir layers have been identified, and key petrophysical input parameters have been obtained for the San Andres and Mississippian study areas.

Accomplishments for this reporting period are detailed below.

2.0 RESERVOIR CHARACTERIZATION STUDIES

During the October 2005 – March 2006 reporting period, significant progress was made in the reservoir characterization studies for all three of the study areas. Parameters obtained from these studies will be used to populate geomodels for reservoir simulation.

2.1 Permian San Andres Study Area

The Permian San Andres (Figure 2.1.1) study area is approximately 5 square miles (13 square kilometers) in size and covers the “High Volume Area” of Waddell Field, Crane County, Texas (Figures 2.1.2 and 2.1.3). This “High Volume Area” is characterized by variable fluid production, but overall fluid production is an order of magnitude greater than in surrounding areas of the field (Figures 2.1.4 and 2.1.5). Operator-interpreted tracer and pressure data indicate this field is a highly compartmentalized reservoir with an active water drive, and cores from two wells show an anhydrite cemented karst overprint, with evidence of later anhydrite dissolution along fractures connecting the productive reservoir zone with the underlying aquifer; however, conventional seismic data have not revealed fracture or karst system patterns that coincide with production patterns. We hope to use multi-trace seismic attributes, such as volumetric curvature (Al-Dossary and Marfurt, 2006) to improve our interpretation of reservoir compartment boundaries and preferential fluid conduits.

The focus of the San Andres reservoir characterization study during the October 2005-March 2006 reporting period has been in the areas of (1) seismic characterization, to identify seismic attributes that have apparent correlation with compartment boundaries and fluid conduits, and (2) petrophysical characterization, to identify using log data reservoir parameters which will be necessary to populate the geomodel.

Seismic Characterization

During this reporting period, we have attempted to tie features seen on seismic attribute maps with reservoir production and engineering-based interpretations of reservoir compartment boundaries.

In the “High Volume Area”, the seismic reflection corresponding to the top of San Andres (Figure 2.1.3) is a poor reflection, and difficult to interpret. In order to approximate the top San Andres for attribute analysis, we flattened the data on the Grayburg horizon and extracted attributes along a stratal slice 30 ms below the Grayburg. There is no visual correlation between the various seismic attributes that have been plotted for the San Andres (e.g., Figure 2.1.4 and 2.1.5) and either the variable fluid production in the “High Volume Area” or the engineering-based compartment boundaries. However, highest oil production does occur primarily to the west of a high coherence band in the center of the “High Volume Area” (Figure 2.1.4), and the Most Negative curvature map (Figure 2.1.5) shows lineaments that form apparent small compartments, although the significance of these lineaments is not yet understood.

A better tie with the engineering-based compartment boundaries is found in a Most Positive curvature map extracted along a Devonian horizon, approximately 500-600 ms below the San Andres reservoir (Figures 2.1.3 and 2.1.6). This map shows lineaments that appear to truncate at the compartment boundaries in the overlying San Andres. We hypothesize that the tectonic fractures that controlled preferred dissolution of anhydrite cement in the San Andres reservoir have trends that coincide with the lineament trends on the Devonian horizon.

Petrophysical Characterization

Petrophysical studies during this reporting period focused on methods for estimation of porosity and permeability from logs in the San Andres Formation using core and log data from W. N. Waddell #1261 (Figure 2.1.4).

Reliable pore volume determination from logs in the San Andres Formation is complicated by the occurrence of gypsum and anhydrite. Although the overall mineral composition of the San Andres is dominated by dolomite, even small amounts of anhydrite have marked effects on the density log, while the water of crystallization of gypsum causes high apparent neutron porosity readings.

W. N. Waddell #1261 provides an excellent key well for log porosity calibration because it has 89.7 ft (27.3 m) of core with porosity and other petrophysical measurements together with neutron, density, and sonic porosity logs. The cored interval penetrates a karst zone with pore space occluded by anhydrite overlying a porous oolite shoal development that contains variable amounts of gypsum. In the following analysis, the core data were first depth-shifted to match log depths from a comparison of core gamma measurements and porosity variability with their log equivalents.

Neutron-density log porosity computation

In carbonates composed of varying amounts of dolomite and limestone, the use of the neutron and density porosities in combination, either as a cross-plot porosity or a simple average generally serves as a reasonable estimate of volumetric porosity measured in core. The overlay of crossplot and average neutron-density log porosities on core porosity measurements (Figure 2.1.7) shows clearly the anhydrite and gypsum effects. In the upper part, anhydrite within the karst zone causes the neutron-density average to read negative porosity because of the high density of anhydrite. The algorithm of the crossplot porosity is an improvement but systematically overestimates the core porosity by a small amount. In the lower, oolite shoal zone, both the crossplot and average neutron-density porosities significantly overestimate core porosities because of the gypsum content in this facies. The presence of gypsum in this zone is confirmed both by visual observation and differences between high- and low-temperature core porosity measurements.

Compositional log analysis of porosity

For many years, estimations of porosity in reservoirs with complex mineralogies have been resolved by a computer-driven multimineral petrophysical model that calculates mineral proportions and volumetric porosity simultaneously. Perhaps the original

published example of this approach was developed in the San Andres Formation by Alger et al. (1963), who computed proportions of dolomite, anhydrite, gypsum, and porosity from a neutron, density, and sonic log combination. The introduction of the photoelectric factor measurement has provided a better solution, particularly because the sonic log is largely insensitive to vugs and oomoldic porosity development within the San Andres Formation.

Compositional analysis of the cored interval of the San Andres Formation in W. N. Waddell #1261 was made using the density, neutron porosity, and bulk photoelectric factor (the product of the density and photoelectric factor) logs to solve for proportions of dolomite, anhydrite, gypsum, and porosity (Figure 2.1.8).

Incorporation of the sonic log for the partition of porosity

The sonic log is a good measure of interparticle porosity, but is largely insensitive to larger pores that occur as vugs or oomolds. The compositional solution for the San Andres Formation in W. N. Waddell #1261 was used to compute a variable matrix transit time, using weights that matched the proportions of dolomite, anhydrite and gypsum. This estimate of sonic-derived porosity is shown together with the porosity from the compositional analysis and core measurements of porosity (Figure 2.1.9).

The porosity estimated from compositional analysis represents a volumetric measure of porosities of all kinds and shows a good concordance with core data. The sonic porosity is a close match with compositional porosity in zones where all the pore space is probably interparticle, but shows distinctive deviations in higher porosity zones where part of the pore space is vuggy or oomoldic. In the karst zone, the sonic porosity suggests that the low pore volumes are dominated by vugs. In the oolite shoal, the higher porosity developments appear to be about equally divided between interparticle and oomoldic pore space.

Estimation of permeability in the San Andres from logs

The prediction of permeability in carbonates based on logs is particularly challenging because of the major role of pore-size in addition to pore volume. In addition, even when the pore-size distribution can be characterized effectively, useful predictive relationships are most commonly based on interparticle porosity, because vugs (represented in the San Andres Formation of the Waddell Field both by dissolution within the karst zone and oomolds within the oolite shoal) contribute little additional permeability. Also, potential increases in permeability attributed to fractures will be difficult to accommodate in log transform predictions because fracture porosity is typically small in volume.

The crossplot of Figure 2.1.10 shows core total porosity versus permeability differentiated between the karst and oolite shoal zones. The two data clouds show an overall concordant trend although some high permeability outliers within the karst zone suggest fracturing, while variations in oomoldic porosity probably cause the expanded range in porosity at different porosity levels.

Because the porosity transform of the sonic log appears to be a good estimator of interparticle porosity, core permeabilities were plotted against sonic porosity (Figure 2.1.11). The crossplot shows that almost all points for both karst and oolite shoal zones occur within the Lucia petrophysical large-particle class (Lucia, 1995), which also matches core descriptions of grainstone facies. If the facies in this well are representative of San Andres facies within the study area, then this observation could simplify permeability prediction to a single particle class transform. The use of the sonic porosity log as interparticle pore volume estimator also appears to tighten the permeability porosity trend as compared with core porosity measurements, which include both interparticle and vuggy pores. Consequently, methods for prediction of permeability in other, uncored wells should incorporate distinctions between pore types wherever possible.

Application of these results to other wells in the Waddell Field Study area

W. N. Waddell #1261 provides an excellent “keystone” well because of its extensive log suite, core measurements, and proven congruence between log estimates and core measurements of porosity. Only one other well has core data, and the well set as a whole has a variety of logs of different vintages. Consequently, the evaluation of different algorithms for porosity estimations from diverse logs will be applied as tests to the W. N. Waddell #1261, so that both error envelopes and biases can be examined systematically. In addition, a variety of permeability prediction methods will be evaluated that link core measurements to logs for permeability estimated in wells that have been logged but which lack core. The collective results will be used as porosity and permeability inputs to the Waddell Field geomodel.

2.2 Mississippian Study Area

Reservoir characterization of the Mississippian Spergen reservoir (Figure 2.2.1) in the Cheyenne Wells and Smoky Creek Fields, Cheyenne County, Colorado (Figure 2.2.2) is nearing completion and we are currently defining parameters for input into a geomodel.

Geological Characterization

Regional Geological Setting

The Cheyenne Wells and Smoky Creek fields are located near the crest of the north-northeast-trending Las Animas Arch in eastern Colorado (Fig. 2.2.2). The Las Animas Arch is noted for its long, episodic history of tectonism, ranging from late Paleozoic deformation to Laramide (latest Cretaceous to Eocene) uplift (Maher, 1945).

Subaerial exposure of Meramecian carbonates due to late Mississippian to early Pennsylvanian uplift resulted in a paleotopographic karst valley-ridge system in eastern Colorado (Askew and Humphrey, 1996). In the study area, the St. Louis Formation is subjacent to the basal Pennsylvanian unconformity. The top of the Spergen reservoir interval is approximately 75 ft (23 m) beneath the unconformity surface but, nonetheless, may have been affected by karst. In particular, deep-seated regional fractures that controlled karst development may be present in the Spergen. These fractures may have

been related to movement on the paleo-Las Animas Arch. Other regional structural trends in the vicinity of the study area that may have influenced karst development include a N60E-trending Precambrian shear zone and a N34W-trending high-angle basement fault (Fig. 2.2.2) interpreted by Sims et al. (2001) from an aeromagnetic anomaly map of Colorado (Oshetski and Kucks, 2000).

Structure and Isopach Maps

Formation tops for the wells in the study area were used to generate structure and isopach maps for the Mississippian Spergen, Mississippian St. Louis, and basal Pennsylvanian Keyes Formations (Figures 2.2.3 - 2.2.6). A structurally high area in the western portion of the Cheyenne Wells and Smoky Creek fields appears to be bounded by a Precambrian shear zone and a high-angle basement fault identified by Sims et al. (2001), and a structurally low area to the south of the fields appears to be bounded by the high-angle basement fault. Spergen production sits on a local structural high with an apparent overall northeasterly trend in the Cheyenne Wells field and a north to northwesterly trend in the Smoky Creek field. On this high, there are coincident local depressions on the top Spergen, top St. Louis (corresponding to the basal Pennsylvanian unconformity surface), and top Keyes structure maps, with diameters of perhaps 0.5 mile (0.8 km) and relative depths of up to approximately 66 ft (20 m) on the top Spergen and top St. Louis maps, decreasing to 57 ft (17 m) on the top Keyes map. The coincidence of local thicks on the Keyes isopach map with the local depressions on the St. Louis structure map (Figure 2.2.4) indicates that the depressions were present during deposition of the basal Pennsylvanian Keyes Formation. The depressions are interpreted as karst features that formed during pre-Pennsylvanian exposure of the Mississippian carbonates.

The Spergen varies from 51 to 116 ft (16 to 35 m) in thickness in the study area, with the thickest Spergen occurring in a northwest-trending band covering the eastern portion of Cheyenne Wells field (Figure 2.2.6). The distribution of Spergen producers versus dry holes on the structural high is not directly related to structure or thickness of the Spergen, indicating that local variation in rock properties and/or fracturing play a significant role in production.

Wireline Log Stratigraphic Interpretation

From log response, the Spergen can be divided into three intervals (A, B, and C) (Fig 2.2.7 and 2.2.8), which are correlatable field-wide. All of these zones produce oil.

Core Description

Core description for the cores within the study area has been completed and interpretations augmented by results of thin section analysis.

There are two cores available in the study area (Figures 2.2.3-2.2.6). These cores have been described using a digital format created by KGS research staff (Dubois et al., 2003). This digital description includes rock type, Dunham/Folk classification, amount of argillaceous material, initial grain size, main pore type, subsidiary pore types, crystal size, bedding, fauna, color, presence of glauconite, pyrite, anhydrite nodules, and oil

staining, whether dolomite is sucrosic or not, and if fractures present are cement filled (Figures 2.2.7 and 2.2.8).

Core description reveals a complex history for the reservoir. Based on faunal and lithofacies assemblages, the depositional environment is interpreted to be on a normal marine shelf with a migrating shoal. Lithofacies range from mudstone to grainstone; however, the entire section has been heavily dolomitized, obscuring most primary depositional structures. Porosity is mainly intercrystalline, intergranular, and moldic. In the productive zones, porosity is mainly moldic and intergranular in the form of solution enhanced voids. Moldic porosity is mostly of foraminifera, crinoids, and bryozoans. Fractures identified in the cores are mostly filled with calcedony, megaquartz, and baroque dolomite.

The two cores show that there is a variation in lithologies and in the depositional and diagenetic signatures of the Spergen across the study area. Significantly more organic-rich mudstone is present in the Klepper #4 core than in the Champlin Aldrich #3 core. This organic-rich mudstone can be identified on logs and the variation in its thickness can be seen in other wells across the field. The amount of organic-rich mudstone apparently has no effect on production.

The quality of the producing zones within the Spergen in the Klepper #4 and Champlin Aldrich #3 is also evident from the core analysis. The Klepper #4 producing zone is a higher quality, having larger and more well connected pores, even though the Champlin Aldrich #3 has more moldic porosity and fractures. The production history of the two wells (Table 2.1) is consistent with this observation.

Thin Section Description

Two hundred representative samples of Spergen were taken from the two cores and made into 1 in. x 2 in. (2.5 cm x 5.1 cm) thin sections. Ninety-four thin sections were stained using the Dickson Formula (1965). This formula uses Potassium ferricyanide and Alizarin Red S to help differentiate between calcite and dolomite. It will also differentiate between high and low iron content within the calcite and dolomite. Calcite will turn pink to purple, with respect to low or high iron content, and dolomite will either stay colorless (no iron) or turn a turquoise blue (high iron content). The staining revealed a few 1 in. (2.5 cm) to 2 in (5.1 cm) intervals within each core containing calcite. These intervals (referred to here as dolo-limestones) occur at a range of depths. No iron was present in either the dolomite or the calcite.

Thin section observations (Figures 2.2.9 and 2.2.10) reveal a complicated paragenesis for the Spergen. The hypothesized sequence is as follows: 1) Deposit mudstone to fossiliferous grainstone in a migrating shoal. 2) Begin first episode of dolomitization. During this episode of dolomitization, porosity development was induced by solution enhancement of voids and fossils. 3) Begin precipitation of calcedony into fractures and voids due to an increase in heat and amount of fluids circulating through the system. It is not clear if the calcedony is also a replacive mineral. 4) Precipitate megaquartz and anhydrite. 5) Precipitate baroque dolomite. This is the last episode of dolomitization

present in the two cores. Megaquartz and baroque dolomite are commonly hydrothermal precipitants. It is likely that activity associated with the Las Animas Arch introduced the hydrothermal saline high calcite and sulfate fluids into the area and influenced the megaquartz and baroque dolomite precipitation.

Core Petrophysical Characterization

In the November 2005 semi-annual scientific/technical report, there was a question about whether the full-diameter core data from Champlin Aldrich #3 and the core plug data from Klepper #4 could be reliably combined for analysis of permeability-porosity trends in the Cheyenne Wells field. Therefore, during the October 2005-March 2006 reporting period, 69 core plug samples were taken from the Champlin-Aldrich #3 core and permeability (k) and porosity (ϕ) were measured. Comparison of full-diameter and plug permeability-porosity trends (Figure 2.2.11) show that the data are consistent and indicates that fracturing plays little role in permeability at this scale. Differences between plug and full-diameter permeabilities (Figure 2.2.12) reflect effects of confining stress difference.

Lithofacies, Permeability, and Porosity

Lithofacies and early diagenesis are major controls on k and ϕ , despite complex diagenetic overprinting. k and ϕ decrease with decreasing grain/mold size from packstone to mudstone, which is a trend also exhibited by other Mississippian carbonates.

Figure 2.2.13 shows the permeability-porosity trend for all lithofacies for the two cores from Cheyenne Wells field, along with data from six Mississippian fields in Kansas (Bhattacharya et al., 2005). The permeability-porosity relationship is approximately bounded within 2.5 orders of magnitude by trend lines defined by:

$$\begin{aligned}\log k_{in\ situ} &= 0.25 \phi_{in\ situ} - 2.2 \\ \log k_{in\ situ} &= 0.25 \phi_{in\ situ} - 4.9\end{aligned}$$

Between these bounding trends, each lithofacies generally exhibits a unique range of k and ϕ , with k decreasing with decreasing grain/mold size for any given ϕ . For the Cheyenne Wells field, the relationship between k and ϕ for each lithofacies can be represented by a power-law function of the following form:

$$k_{in\ situ} = A\phi^B$$

where $A=3 \times 10^{-6} \text{ to } 6 \times 10^{-3}$ and $B \approx 3.45$, and where Lith represents an integer classification of the lithofacies (0-mudstone, 1-mud-wackestone, 2-wackestone, 3-wacke-packstone, 4-packstone, 5-pack-grainstone) (Figure 2.2.14). Permeability values for the Champlin Aldrich #3 and Klepper #4 wells are similar at any given porosity except for some mudstone-wackestone and wackestone samples. The significantly better permeabilities of the Champlin Aldrich #3 samples may result from improved moldic porosity connectivity. This is still under investigation.

Permeability and Pore Throats

Although permeability is shown to correlate with porosity, variables that control permeability in Mississippian rocks include pore throat size and distribution, grain size distribution, moldic pore size and packing, and moldic pore connectivity. Porosity is only one of the variables controlling permeability and bivariate correlation therefore relies on the correlation between porosity and the other controlling variables. A crossplot of permeability and principal pore throat diameter (PPTD) illustrates the control PPTD exerts on permeability (Figure 2.2.15). Two samples from the Champlin Aldrich #3, a mudstone-wackestone ($k=0.0025$ md *in situ* air, $k = 0.0007$ md *in situ* Klinkenberg) and packstone ($k=5.67$ md *in situ* air, $k = 4.66$ md *in situ* Klinkenberg) exhibit PPTD consistent with other rocks, including Mississippian rocks. Pore throat size distributions are consistent with unimodal distribution (Fig. 2.2.16), indicating that moldic porosity is only accessed through matrix porosity.

Capillary Pressure

Capillary pressures and corresponding water saturations (S_w) vary among lithofacies, and with porosity/permeability and gas column height. Threshold entry pressures and corresponding heights above free water level are well correlated with permeability and consistent with the relationship between pore throat size and permeability. Capillary pressure curves for a mudstone-wackestone and packstone illustrate approximate upper and lower limits for rocks from the Cheyenne Wells field (Fig 2.2.17). Permeable packstones exhibit sufficiently low entry pressure (and equivalent oil column height) that these rocks are able to achieve water saturations of less than 50%, but significant portions of the reservoir are in the transition zone. Oil column heights are insufficient to enter low permeability mudstones and these rocks are water saturated ($S_w=100\%$).

Core to Log Comparison

Petrophysical log properties are correlated to core data to allow for better prediction of petrophysical properties in non-cored wells.

Compositional analysis using wireline log data allows us to independently estimate the mineral composition of the rocks. Results can be compared to lithologies from core descriptions to test whether the log data provides a realistic representation of the rocks. We use an Excel spreadsheet to set up the matrix algebra solution for compositional analysis. The MINVERSE function within Excel is used to perform the operation through inversion of the matrix of the log properties of the components. The logs used in the composition analysis are: gamma ray, neutron porosity (percent), bulk density, and photoelectric volumetric cross section. By premultiplying the logs by this inverse matrix, we can determine the percentage of calcite, dolomite, quartz, shale, and porosity. Results for the Champlin Aldrich #3 and Klepper #4 wells (Figure 2.2.18) demonstrate that mineral compositions estimated from the logs show good concordance with lithologies described from core. The composition graph is a useful quantitative representation of lithofacies, porosity, and amount of dolomitization observed within each core.

Porosities from neutron and density logs were averaged to remove lithology effects and normalized (see following *Log Petrophysical Characterization* section), and the resulting neutron-density log porosities were compared to core helium porosities from the Champlin Aldrich #3 and Klepper #4 wells. In Klepper #4, the core porosity is from plugs. In Champlin-Aldrich #3, both whole-core and plug porosity is plotted and compared with log porosity. For both wells, the log and core porosity data have similar values overall (Figure 2.2.19), showing that the log data is well-calibrated and a good approximation of the rock characteristics, although there is a discrepancy between the two datasets in the vicinity of the perforated interval in Klepper #4, with the core porosity higher than the log porosity by up to 5 porosity units. This discrepancy is most likely due to the preferential selection of plugs with highest porosity for analysis.

Log Petrophysical Characterization

In order to ensure that neutron-density log porosities were normalized between the 18 wells in the study area with neutron-density logs, average neutron porosity and average density porosity were calculated for an approximately 735 ft (224 m) interval between the Shawnee and Cherokee formation tops (Figure 2.2.1) in each well. Based on these results, a correction was applied to the neutron-density porosity for each well. The maximum neutron-density porosity correction was 1.4 porosity units.

Modified Pickett crossplots were created in the PffEFFER software (Doveton et al., 1996) using digital log data. These Pickett crossplots were used to analyze patterns in porosity, resistivity, and saturation in the reservoir. Each data point on these plots represents a half-foot interval and points are linked together in sequence by depth to reveal trends through the reservoir. From the Archie relations, saturation (S_w) contours and bulk volume water (BVW) contours are superimposed. Details of the methodology in using the modified Pickett plots are described in Doveton et al. (1996). Inputs for the program are: wireline log resistivity and porosity, water salinity, and Archie parameters (m and n). The Pickett plots from Champlin Aldrich #3 (Figure 2.2.20) reveal a distinct pattern of increasing BVW from Spergen zone A to Spergen zone C. Spergen Zone A has an approximate BVW cutoff of 0.03, Spergen Zone B a BVW cutoff of 0.045, and Spergen Zone C a BVW cutoff of 0.06. Similar patterns are also seen in other wells. This corresponds with the hypothesis that the Spergen reservoir is a bottom water drive system. Porosity, BVW, and permeability cut-offs were used to identify the net pay at each logged well in the study area and to identify potential bypassed pay.

Engineering Characterization

Lease production data for the Cheyenne Wells and Smoky Creek fields have been assigned to individual wells and production history of the wells has been examined. Completion dates are primarily either in the 1970's or the 1990's. In order to compare production performance between wells with such a wide range of completion dates, we have calculated the production from the first 60 months of a well's history. Well performance in the Cheyenne Wells and Smoky Creek Fields is extremely variable, with a wide range in oil cumulatives (Fig 2.2.21). Based on calculations from matrix porosities

alone, some wells have performed better than expected, while others have under performed. For example, comparing the Crosby #2, Crosby #3, Klepper #4, and Champlin Aldrich #3 wells (Table 2.1 and Figure 2.2.22), all completed in the early 1990's, we see variability in production that appears to have little relationship to matrix porosity. Fractures are believed to contribute to this variability.

Seismic Characterization

Structure

As was reported in the November 2005 semi-annual scientific/technical report, the St. Louis, Spergen and Warsaw formation tops do not correspond to significant acoustic impedance contrasts. The closest seismic horizon to the Spergen reservoir that can be reliably interpreted across the entire 3-D seismic dataset is the top Keyes. A subsea depth structure map (Figure 2.2.23) of this surface has been constructed from the top Keyes time structure map using a velocity grid computed from data at well locations. The drainage pattern interpreted on this structure map is reminiscent of karst drainage consisting of blind valleys, and local topographic depressions as small as 20 acres (80,930 square meters) in size may be sinkholes. This evidence for karst is consistent with interpretations of the structure and isopach maps from well control; however, the seismically-derived structure map provides more details about the topography of the top Keyes surface than is possible with well control alone. Another significant feature appearing on the top Keyes seismic structure map is a N60E-trending down-to-the-south fault at the southern end of the seismic survey, which aligns with a Precambrian shear zone. This suggests that the fault is a reactivation of a Precambrian zone of weakness.

A deeper continuous horizon (approximately 50-60 ms below the top Keyes) corresponding to an impedance increase and tentatively interpreted as the top of Kinderhook has been interpreted across the seismic survey. It is assumed that features (e.g., structural highs, lineaments, etc.) evident on both this horizon and the top Keyes horizon will be present within the intervening Spergen reservoir interval.

The positions of the top and base of the Spergen in the seismic data volume are approximated using the top Keyes horizon and isochron maps calculated from isopach maps and interval velocities from wells with sonic logs.

Attribute Analysis

Average acoustic impedance for the interval between the top and base of the Spergen has been extracted from the model-based inversion volume that was generated during the previous reporting period (Fig. 2.2.24). The average acoustic impedance map clearly shows spatial variation, with broad northeast-trending bands of high and low impedance. Variation in acoustic impedance can be an indicator of porosity variation. In order to test whether there is a relationship between acoustic impedance and porosity in the Spergen reservoir, acoustic impedance has been extracted at well locations and crossplotted against porosities obtained from well logs (Fig. 2.2.25). The crossplot shows considerable scatter, but in general, there is a trend indicating that higher acoustic impedance corresponds to lower porosity.

Extractions from the Most Negative curvature and Most Positive curvature volumes have been made along the top Keyes and hypothesized Kinderhook horizons (Figure 2.26). Several sets of large scale high curvature lineaments have been interpreted from these maps. The curvature lineaments show orientations that parallel basement structural orientations, as well as the Las Animas Arch. Interpreted curvature lineaments may reflect subtle structural features, fractures or reservoir compartment boundaries that are the cause of the production inconsistencies in the Cheyenne Wells and Smoky Creek fields.

2.3 Arbuckle Study Area

The primary Arbuckle study area, in Russell County, Kansas, is a 10 mi² (26 km²) area covered by a 3-D seismic survey. In this study area, the Arbuckle reservoir sits at or near a pre-Pennsylvanian unconformity and karst surface (Figure 2.3.2). Arbuckle production is located on local remnant highs (Figure 2.3.3); however, not all wells drilled on the Arbuckle highs are productive. Reservoir quality is variable, and reservoir characterization focuses on distinguishing tight Arbuckle from porous Arbuckle, as well as identifying the locations of the local structural highs.

Geological Characterization

A regional characterization of the Arbuckle erosional surface for an 1800 mi² (4662 km²) area covering Russell and Barton counties and centered on the seismic study area has been conducted in order to characterize the regional geomorphology of the Arbuckle karst surface (Figure 2.3.1). This study complements work conducted by Cansler (2001) in Barton, Ellsworth, Rice, and northern Stafford counties, which revealed two types of Arbuckle erosional terrain: polygonal karst and groundwater-sapped plateaus. Significantly, Cansler (2001) concluded that differences in oil productivity can be recognized between the two terrains.

Extending our study area to include all of Russell and Barton counties allows an overview of the Arbuckle structure across the entire Central Kansas Uplift (Figure 2.3.4). At the time of the November 2005 semi-annual scientific/technical report, only preliminary maps of the Arbuckle surface had been made. Since then, nearly all of the 16,000 Arbuckle tops in Russell and Barton Counties have been screened, and several more logs have been scanned into the study area. Gridding algorithms have been refined to map the most accurate, yet detailed, topography of the Arbuckle surface.

The Arbuckle surface in Russell and Barton counties appears to be dominated by groundwater-sapped plateaus, half-blind valleys, and polygonal karst (Figure 2.3.5). As suggested in the April 2005 semi-annual scientific/technical report, the 3-D seismic study area exhibits geomorphologies reminiscent of polygonal karst, as can be seen on volumetric curvature extractions along the Arbuckle horizon (Figure 2.3.6).

In areas at the crest of the Uplift, erosional processes have completely removed Arbuckle strata, and Precambrian basement rocks directly underlie Pennsylvanian strata. These exposures of Precambrian basement are interpreted to be along the up-tilted edges of blocks caused by uplift during the Ouachita Orogeny along reactivated basement faults. These blocks dip to the southwest, and show evidence of groundwater sapping updip to the northeast. Evidence for these up-tilted blocks is interpreted from gravity and magnetic lineaments of Precambrian basement rocks in Kansas (Figure 2.3.7).

A regional southwest-northeast-trending cross section has been constructed to demonstrate trends in the Arbuckle surface and overlying strata. The cross section was constructed compiling vast numbers of logs which illustrate the complexity of Pennsylvanian cyclic stratigraphy over the karst topography of the Central Kansas Uplift (Figure 2.3.8). From log data, it appears that the Nuyaka Creek Shale Member of the Marmaton Group (upper Desmoinesian) is the lower-most unit to span the crest of the Uplift. Below the Nuyaka Creek, Pennsylvanian strata onlap the Uplift, except where basal Pennsylvanian conglomerate infills localized topographic lows.

Seismic Characterization

The Arbuckle time structure map constructed during the April to September 2005 reporting period was converted to depth using a velocity grid calculated from Arbuckle formation tops and horizon times at the wells. The Arbuckle depth structure map was gridded at an 82.5 ft (25.1 m) grid size to match the bin size of the seismic data (Figure 2.3.3). The 3-D seismic map shows much more “roughness” in the surface of the Arbuckle than the map constructed from well tops alone. While the seismic data does confirm the overall trend of karst features seen in the original tops map, it does cast doubt on whether the wells, with their sparse horizontal sampling, can give a remotely realistic picture of the roughness of the paleokarst surface.

Roughness is a crucial matter to consider in mapping a karst reservoir. If formation tops are structurally high at two adjacent wells and a smooth surface is mapped between them, most geologists would infer that there are no viable “sweet spots” remaining. If, however, the surface is much rougher than the well data reveals, it is possible, and under certain circumstances, likely, that untapped structural highs exist between the wells.

In order to compensate for this roughness, geostatistical analyses have been employed to estimate the number of possible highs that may exist between well control points. A variogram of the area of seismic data was used to construct a variogram model, which constrained the gridding operation of the tops data using sequential Gaussian simulation (a stochastic simulation) (Figure 2.3.9). This new simulated Arbuckle surface shows approximately the same roughness as the 3-D seismic surface, and a much rougher surface than the tops surface (Figures 2.3.10 and 2.3.11). The following weeks will be dedicated to approximating the probability of the number of structural highs or “sweet spots” existing between known producing wells.

Also, in order to evaluate whether the roughness is similar between areas of polygonal karst and areas with groundwater-sapped plateaus, future work will include determining roughness from a 3-D seismic survey in a groundwater-sapped terrain in Ellis County, KS, and comparing with the results from our seismic survey in Russell County.

Arbuckle Production

Arbuckle production has been plotted by lease for Russell and Barton counties (Figure 2.3.12). Areas of highest production occur along hypothesized up-tilted edges of blocks, where grainier horizons would be preserved from groundwater-sapping processes. Within the seismic survey area, approximately 30 wells have produced from the Arbuckle (Figure 2.3.3), although some of these wells were only marginally productive. In some cases, non-productive wells sit on the same structural highs as wells with Arbuckle production, suggesting local variability in porosity/permeability.

The coming months will focus on assigning lease production to individual wells, estimating trends in porosity from logs, and correlating porosity with annual well production.

3.0 GEOMODEL CONSTRUCTION

Although we have not yet constructed geomodels for the study areas, we have developed a workflow for geomodel building, including a methodology for determining the parameters necessary for populating the geomodels. As has been shown in the reservoir characterization discussion above, several of these parameters have already been obtained for the Permian San Andres and the Mississippian Spergen reservoirs. Also, the Permian San Andres and Mississippian Spergen reservoirs have been divided into major vertical intervals, separated by potential permeability barriers. For the San Andres study area, the reservoir is separated into two intervals, a lower G8 interval and an upper G9 interval (Figure 2.1.1), with the top G8 unconformity surface identified as a potential permeability barrier. For the Mississippian study area, the Spergen reservoir is separated into three intervals, A (top), B (middle), and C (bottom).

Steps for building the geomodel:

- Complete separate Pickett plots for each interval at each well.
- Define best estimates for porosity, gamma, and bulk volume water (BVW) cut-offs.
 - Cut-offs may vary between intervals. – Employ knowledge about regional geology to make choices.
- D&A wells
 - Enter petrophysical cut-offs at each D&A well.
 - Identify net-pay (if any) at each interval at each well.
 - Fine-tune petrophysical cut-offs to obtain zero net-pay at each D&A wells.
 - Justify if net pay is greater than zero. - Justify whether well completion may be the cause.

- Define petrophysical cut-offs that result in negligible net pay at D&A wells.
- Productive wells
 - Employ cut-offs defined using D&A wells at each interval in each productive well.
 - Estimate net-pay feet at each well by adding net-pays in each interval at each well.
- Plot cumulative production against net pay-feet for all productive wells. - Is there a positive correlation between net pay-feet and cumulative production?
- Map net-pay within each interval across the field.
 - Fine tune top and bottom picks of net pay in each interval at each well if necessary.
- Plot permeability vs. porosity data.
- Focus on permeability-porosity data set which qualifies porosity/gamma cut-offs.
 - Discriminate core plugs on basis of gamma or any other available log parameter.
 - Define best correlation to estimate permeability at uncored but logged wells.
- Estimate permeability for each net pay at each well. Map net pay permeability for each interval across field.
- Plot DST recovery and pressures in cross section.
- Identify lowest subsea depth below which DST's always result in water production.
 - Make first estimate of free water level (FWL) subsea depth.
- Plot BVW vs. subsea depth from net pay from each interval at each well.
 - Is there any indication about location of FWL?
 - How close is this FWL to that estimated from DST recovery?
- Make final estimate of field wide FWL(s).
- Based on porosity and permeability distribution for each interval across the field, identify flow-units (layers) for reservoir simulation.
- Map flow-units across field, introducing hypothesized lateral flow barriers interpreted from seismic data.

4.0 TECHNOLOGY TRANSFER

Papers documenting our project results have been presented at national and regional conferences and have been submitted for upcoming conferences.

The following papers were presented at the AAPG Annual Convention, April 9-12, 2006, in Houston, TX and at the 2006 DGGG Expo, May 3, 2006, in Grapevine, TX:

Application of New Seismic Attributes to Identify Karst and Fracture Related Compartmentalization: Permian San Andres Formation, Central Basin Platform, West Texas (USA), by E. C. Sullivan, S. Nissen, K. J. Marfurt, and C. H. Blumentritt

Karst and Fracture Features Affecting Reservoir Performance in a Mississippian Reservoir, Cheyenne County, Colorado, by N. B. Givens and S. Nissen. This paper has also been published as Kansas Geological Survey Open-file Report 2006-14.

The following papers are to be presented at the 26th Annual GCSSEPM Foundation Bob F. Perkins Research Conference, December 3-6, 2006, and have been submitted for publication in the associated proceedings volume.

Application of Volumetric 3-D Seismic Attributes to Reservoir Characterization of Karst-Modified Reservoirs, by C. Sullivan, S. Nissen, and K. Marfurt

An Integrated Study Delineating Karst and Fracture Features Affecting Reservoir Performance in a Mississippian Reservoir, Cheyenne County, Colorado, by N. B. Givens and S. Nissen

In addition, information related to the project (including project background, personnel, a catalog of seismic karst features, publications, and semi-annual scientific/technical reports) is posted to our project website: <http://www.kgs.ku.edu/SEISKARST>.

CONCLUSIONS

San Andres study area:

- Most Positive volumetric curvature extracted 500-600 ms below the San Andres reservoir shows lineaments that appear to truncate at the compartment boundaries in the overlying San Andres. The lineament trends seen on this deeper surface may relate to tectonic fractures that controlled preferred dissolution of anhydrite cement in the San Andres reservoir.
- A compositional model using neutron, density, and photoelectric logs that accommodates gypsum and anhydrite is a good predictor of total porosity in the San Andres.
- Integration of porosity from the sonic log with porosity from compositional analysis allowed partition of the pore space between interparticle porosity and coarser porosity, either as vugs within the karst zone or oomodic porosity in an oolite shoal development.

Mississippian study area

- Core, log, and seismic data provide complementary information about the Spergen reservoir.
- Structure and isopach maps from well data, supplemented by information from 3-D seismic interpretations, indicate karst features on the pre-Pennsylvanian unconformity surface 75 ft (23 m) above the Spergen reservoir.
- Core and log data show that productive Spergen exhibits a variety of lithofacies and a wide range of matrix porosities.
- Core petrophysical analysis reveals a permeability-porosity relationship that is affected by lithofacies.

- Calibration of log properties to core properties in cored wells allows better prediction of petrophysical properties in non-cored wells.
- Acoustic impedance from a seismic inversion volume roughly correlates with log porosity.
- Production is not well correlated with matrix porosity, suggesting that another parameter controls well performance.
- Volumetric curvature extractions along key horizons above and below the Spergen reservoir exhibit lineaments with orientations that parallel regional structural orientations. These curvature lineaments may reflect subtle structural features, fractures or reservoir compartment boundaries that are the cause of production inconsistencies.

Arbuckle study area

- Regional geological characterization of the Arbuckle erosional surface distinguishes between areas of sapped plateaus and polygonal karst.
- Areas of highest Arbuckle production appear to be along up-tilted edges of blocks, where grainier horizons were preserved from groundwater-sapping processes.
- Geostatistical analysis of 3-D seismic data is used to predict roughness of the karst surface in areas where there is no seismic data. This method can be used to high-grade areas of potentially bypassed production trapped in local topographic closures.

A workflow for geomodel construction has been proposed that makes use of core, log, seismic, production, and DST data. This workflow will be employed during the next reporting period to develop integrated geomodels for reservoir simulation of the study areas.

LIST OF TABLES

Table 1.1	Project schedule	30
Table 2.1	Comparison of porosity and production data for four Spergen wells from Cheyenne Wells and Smoky Creek fields	30

LIST OF FIGURES

Figure 1.1	Index map showing locations of study areas	31
Figure 2.1.1	Stratigraphic column for upper Leonardian and lower Guadalupian section in the Permian Basin. After Ruppel and Bebout (2001).....	32
Figure 2.1.2	Time structure at the top of the G4 high frequency surface for a 3-D seismic survey over Waddell Field, Crane County, Texas.....	32
Figure 2.1.3	Top: NNE-SSW seismic section across the Waddell field 3-D seismic survey. Bottom: Most Positive curvature extraction along the Devonian horizon.....	33
Figure 2.1.4	Coherence extraction along the top San Andres for the boxed area in Figure 2.1.3.....	34
Figure 2.1.5	Most Negative curvature extraction along the top San Andres for the boxed area in Figure 2.1.3.....	35
Figure 2.1.6	Most Positive curvature extraction along the Devonian horizon for the boxed area in Figure 2.1.3.....	36
Figure 2.1.7	Neutron-density log porosities versus core porosity in the cored interval of the San Andres Formation in W. N. Waddell #1261.....	37
Figure 2.1.8	Compositional analysis of minerals and pore volume in the cored interval of the San Andres Formation in W. N. Waddell #1261 based on neutron, density, and photoelectric factor logs.....	38
Figure 2.1.9	Compositional pore volume and sonic log porosity versus core porosity in the cored interval of the San Andres Formation in W. N. Waddell #1261	39
Figure 2.1.10	Core porosity and permeability crossplot of the San Andres Formation in W. N. Waddell #1261.....	40

Figure 2.1.11	Sonic porosity and core permeability crossplot of the San Andres Formation in W. N. Waddell #1261.....	40
Figure 2.2.1	Stratigraphic column for Mississippian study area, Cheyenne County, Colorado.....	41
Figure 2.2.2	Map of major structural features of eastern Colorado showing oil and gas fields	41
Figure 2.2.3	Structure map of the top of the Pennsylvanian Keyes Formation	42
Figure 2.2.4	Structure map on top of the St. Louis with isopach of the interval between the top of the Keyes Formation and the top of the St. Louis superimposed.....	42
Figure 2.2.5	Structure map on top of the Spergen.....	43
Figure 2.2.6	Isopach of gross Spergen thickness	43
Figure 2.2.7	Core description of Klepper #4.....	44
Figure 2.2.8	Core description of Champlin Aldrich #3.....	45
Figure 2.2.9	Thin section photomicrograph images from Klepper #4	46
Figure 2.2.10	Thin section photomicrograph images from Champlin Aldrich #3	47
Figure 2.2.11	Graph of permeability versus porosity for plug and full-diameter samples from Champlin-Aldrich #3.....	48
Figure 2.2.12	Graph of in situ plug permeability versus full-diameter air permeability	48
Figure 2.2.13	Graph of permeability versus porosity for all lithofacies for the two cores from Cheyenne Wells field, along with data from six Mississippian fields in Kansas (Bhattacharya et al., 2005)	49
Figure 2.2.14	Graph of permeability versus porosity for different lithofacies from Champlin Aldrich #3 and Klepper #4	49
Figure 2.2.15	Crossplot of principal pore throat diameter versus permeability for two samples from Champlin Aldrich #3 compared to undifferentiated sandstones and carbonates, and differentiated Lansing-Kansas City and Mississippian moldic carbonates from Byrnes et al. (2003).....	50

Figure 2.2.16	Pore throat size distributions for a low permeability mudstone-wackestone and a higher permeability packstone. Both rocks show unimodal distribution.....	50
Figure 2.2.17	Capillary pressure curves for a low permeability mudstone-wackestone and a higher permeability packstone illustrating upper and lower limits for rocks from the Cheyenne Wells field.....	51
Figure 2.2.18	Composition graphs for Champlin Aldrich #3 and Klepper #4 created from wireline log data using a matrix algebra solution in Excel	52
Figure 2.2.19	Graph of average neutron-density log porosity and core helium porosity versus depth in Champlin Aldrich #3 and Klepper #4.....	53
Figure 2.2.20	Pickett plots for Spergen A, B, and C intervals in Champlin Aldrich #3	54
Figure 2.2.21	Bubble map showing with red circles the relative amount of oil produced from the Spergen during the first 60 months of production for each well	55
Figure 2.2.22	Comparison of production profiles for four Spergen wells in the Cheyenne Wells and Smoky Creek fields.....	55
Figure 2.2.23	Top Keyes subsea depth structure map derived from seismic data	56
Figure 2.2.24	Average acoustic impedance for the Spergen interval from a model based inversion volume.....	57
Figure 2.2.25	Crossplot of wireline log porosity versus acoustic impedance extracted from the model-based inversion volume	58
Figure 2.2.26	Most Positive and Most Negative curvature extractions along the Top Keyes and Kinderhook horizons	59
Figure 2.3.1	Map of Kansas showing location of regional Arbuckle study area covering Russell and Barton counties.	60
Figure 2.3.2	Stratigraphic column for the Arbuckle study area in Russell County, Kansas, showing Pennsylvanian strata discussed in this report.	60
Figure 2.3.3	Arbuckle structure map depth-converted from 3-D seismic horizon time interpretation.	61

Figure 2.3.4	Arbuckle surface over the Central Kansas Uplift in the study area including Russell and Barton Counties	62
Figure 2.3.5	Detail of Arbuckle surface showing karst features	63
Figure 2.3.6	Volumetric Most Positive curvature extracted along the Arbuckle horizon from the Russell County, Kansas, 3-D seismic survey showing a network of polygonal features reminiscent of polygonal or cockpit karst.....	64
Figure 2.3.7	Arbuckle surface with magnetic and gravity lineaments	65
Figure 2.3.8	West to east cross section across Central Kansas Uplift showing onlapping of Pennsylvanian strata	66
Figure 2.3.9	Variogram from seismic data and model	67
Figure 2.3.10	3-D image of simulated roughened surface of the Arbuckle for Russell and Barton Counties	67
Figure 2.3.11	Close-up of roughened surface of Arbuckle looking along the crest of the Central Kansas Uplift	68
Figure 2.3.12	Arbuckle cumulative production data bubbles on washed-out Arbuckle structure background.....	69

REFERENCES

- Al-Dossary, S., and K. J. Marfurt, 2006, Volume based estimates of spectral curvature: To appear in Geophysics.
- Alger, R.P., L.L. Raymer, W.R. Hoyle, and M.P. Tixier, 1963, Formation density log applications in liquid-filled holes: SPE Transactions of the AIME, v. 228, no. 3, p. 321 – 332.
- Askew, R. L., and J. D. Humphrey, 1996, End-Mississippian paleotopography and interpreted drainage patterns: Eastern Colorado (abstract): AAPG Bull., v. 80, p. 966.
- Bhattacharya, S., M. K. Dubois, A. P. Byrnes, S. E. Nissen, T. R. Carr, E. K. Franseen, M. Shreve, S. Anderson, P. M. Gerlach, and B. Knoll, 2005, Field demonstration of horizontal infill drilling using cost-effective integrated reservoir modeling--Mississippian carbonates, central Kansas: Kansas Geological Survey Open-file Report 2005-28, http://www.kgs.ku.edu/PRS/publication/2005/OFR05_28/index.html.
- Byrnes, A. P., E. K. Franseen, W. L. Watney, and M. K. Dubois, 2003, The role of moldic porosity in Paleozoic Kansas reservoirs and the association of original depositional facies and early diagenesis with reservoir properties: Kansas Geological Survey Open-file Report 2003-32, <http://www.kgs.ku.edu/PRS/publication/2003/ofr2003-32/index.html>.
- Cansler, J. R., 2000, Paleogeomorphology of the sub-Pennsylvanian unconformity on the Arbuckle Group (Cambrian-Lower Ordovician), M.S. thesis: University of Kansas, Lawrence, 123 p.
- Dickson, J. A., 1965, A modified staining technique for carbonates in thin section: Nature, February 6, 1965, p. 587.
- Doveton, J.H., W.L. Guy, W.L. Watney, G.C. Bohling, S. Ullah, and D. Adkins-Heljeson, 1996, Log Analysis of petrofacies and flow-units with microcomputer spreadsheet software: 1995 American Association of Petroleum Geologist Mid-Continent Meeting Transactions, p. 224-233.
- Dubois, M. K., A. P. Byrnes, G. C. Bohling, S. C. Seals, and J. H. Doveton, 2003, Statistically-based lithofacies predictions for 3-D reservoir modeling: examples from the Panoma (Council Grove) Field, Hugoton Embayment, Southwest Kansas: Kansas Geological Survey Open-file Report 2003-30, <http://www.kgs.ku.edu/PRS/publication/2003/ofr2003-30/index.html>.
- Lucia, F.J., 1995, Rock-fabric/petrophysical classification of carbonate pore space for reservoir characterization: AAPG Bull., v. 79, no. 9, p. 1275 – 1300.

Maher, J. C., 1945, Structural development of Las Animas arch, Lincoln, Cheyenne, and Kiowa Counties, Colorado: Geological Notes: AAPG Bull., v. 29, no. 11, p. 1663-1667.

Oshetski, K. C., and R. P. Kucks, 2000, Colorado aeromagnetic and gravity maps and data: a Web site for distribution of data: USGS Open File Report 2000-42, <http://pubs.usgs.gov/of/2000/ofr-00-0042/colorado.htm>.

Ruppel, S. C., and D. G. Bebout, 2001, Competing effects of depositional architecture and diagenesis on carbonate reservoir development: Grayburg Formation, South Cowden field, west Texas: The University of Texas at Austin, Bureau of Economic Geology Report of Investigations No. 263, 62 p.

Sims, P. K., V. Bankey, and C. A. Finn, 2001, Preliminary Precambrian basement map of Colorado – A geologic interpretation of an aeromagnetic anomaly map: USGS Open-File Report 01-0364, http://pubs.usgs.gov/of/2001/ofr-01-0364/colo_of_text.html.

Task Description	FY05				FY06				FY07			
	Oct 04	Jan 05	Apr 05	Jul 05	Oct 05	Jan 06	Apr 06	Jul 06	Oct 06	Jan 07	Apr 07	Jul 07
Task 1.0 Obtain 3-D seismic, geologic, petrophysical, and engineering data	█											
Task 2.0 Generate volumetric attributes												
Task 2.1 Generate attributes for Permian San Andres data		█										
Task 2.2 Generate attributes for Mississippian data		█	█									
Task 2.3 Generate attributes for Arbuckle data			█	█								
Task 3.0 Generate preliminary seismic attribute catalog of karst features												
Task 4.0 Perform reservoir characterization studies												
Task 4.1 Seismic characterization		█	█	█	█	█	█					
Task 4.2 Geologic characterization		█	█	█	█	█	█					
Task 4.3 Petrophysical (log and core) characterization		█	█	█	█	█	█					
Task 4.4 Engineering characterization		█	█	█	█	█	█					
Task 5.0 Construct integrated 3D reservoir geomodels												
Task 6.0 Conduct reservoir simulations												
Task 7.0 Synthesize best practices workflow												
Task 8.0 Model new well paths												
Task 9.0 Drill, log and core new wells												
Task 10.0 Calibrate attributes and reservoir models with new well data; review and refine attribute-based workflows												
Task 11.0 Rerun reservoir simulations with adjusted parameters												
Task 12.0 Finalize seismic attribute catalog and best practices workflows												
Task 13.0 Technology transfer												

Table 1.1. Project schedule. Gray boxes show planned project status. Black boxes show actual project status as of March 31, 2006.

Well Name	Completion Date	Perf Interval Porosity	# of Feet Perforated	60 Month Oil Cum (Bbls)	Total Oil Production Cum (Bbls)
Crosby #2	12-20-1992	7.6%	5	65,359	97,806
	3-29-2000	9.6%	4		
Crosby #3	8-15-1993	11.6%	10	137,975	208,977
Klepper #4	6-28-1993	12.1%	8	42,875	93,910
	10-9-1996	8.4%	5		
Champlin Aldrich #3	8-6-1991	12.8%	8	34,387	91,434
	4-24-1996	9.6%	16		

Table 2.1. Comparison of porosity and production data for four Spergen wells from Cheyenne Wells and Smoky Creek fields.



Figure 1.1. Index map showing locations of study areas.

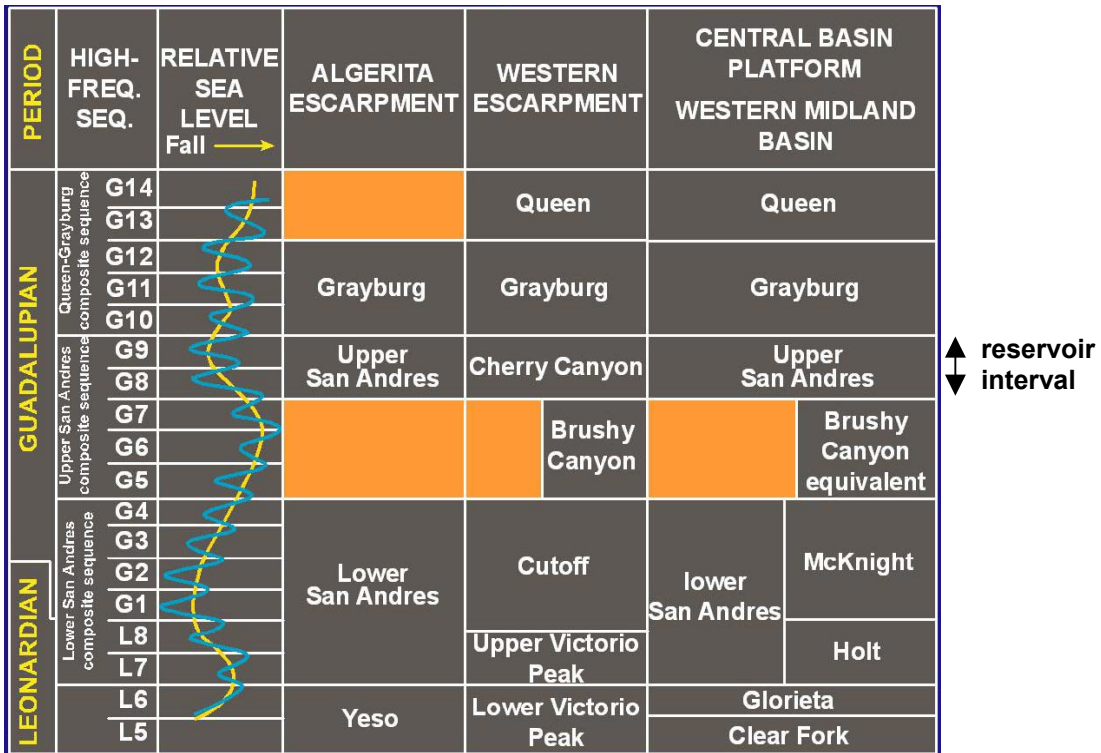


Figure 2.1.1. Stratigraphic column for upper Leonardian and lower Guadalupian section in the Permian Basin. After Ruppel and Bebout (2001).

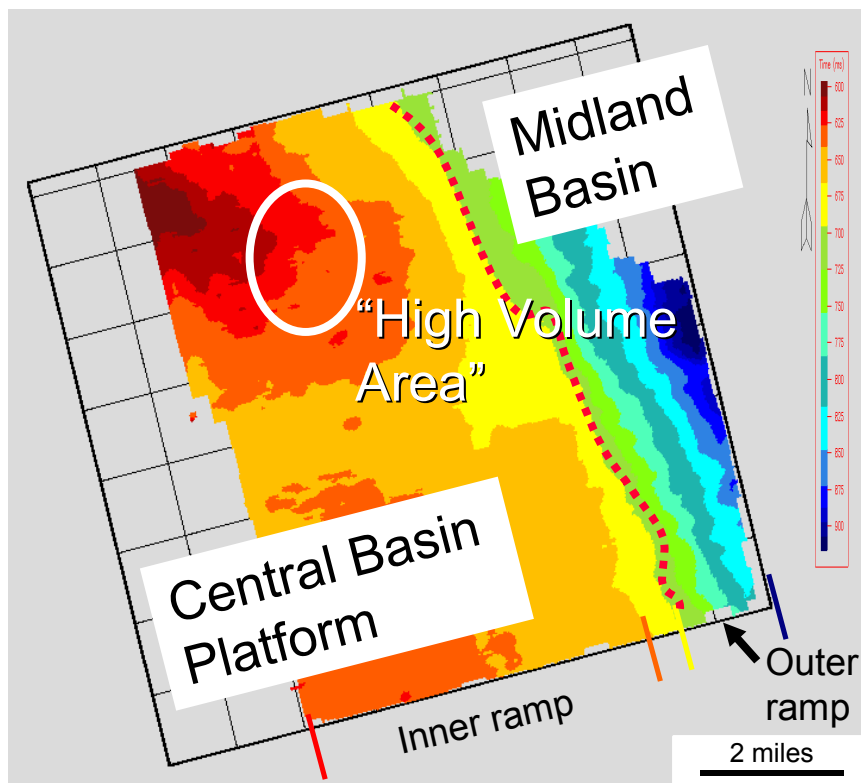


Figure 2.1.2 Time structure at the top of the G4 high frequency surface for a 3-D seismic survey over Waddell Field, Crane County, Texas. Our study area, the “High Volume Area” is outlined in white.

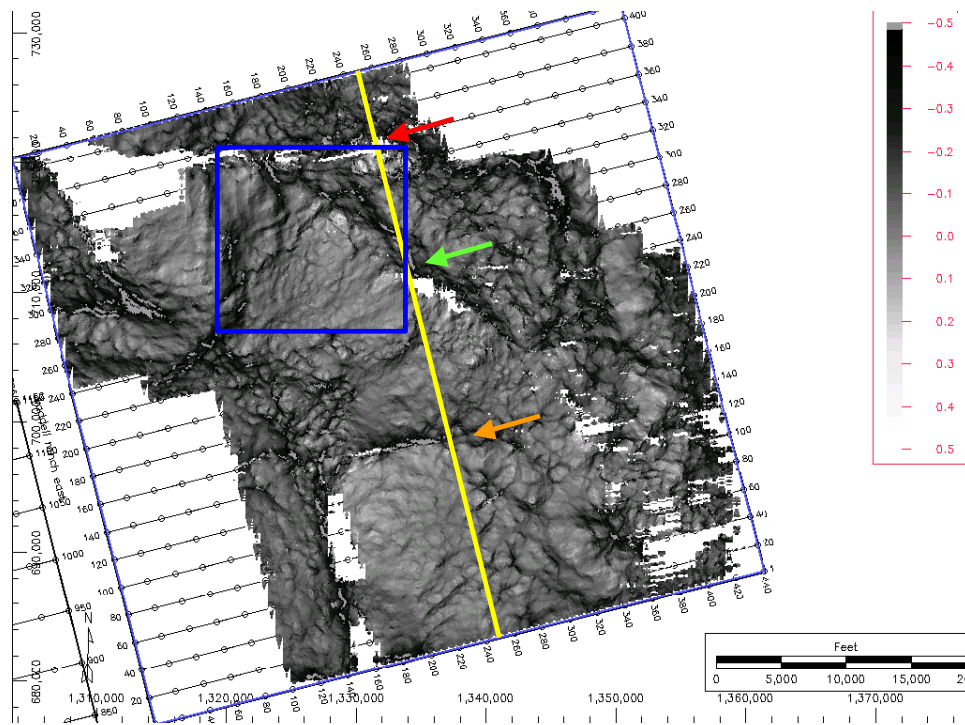
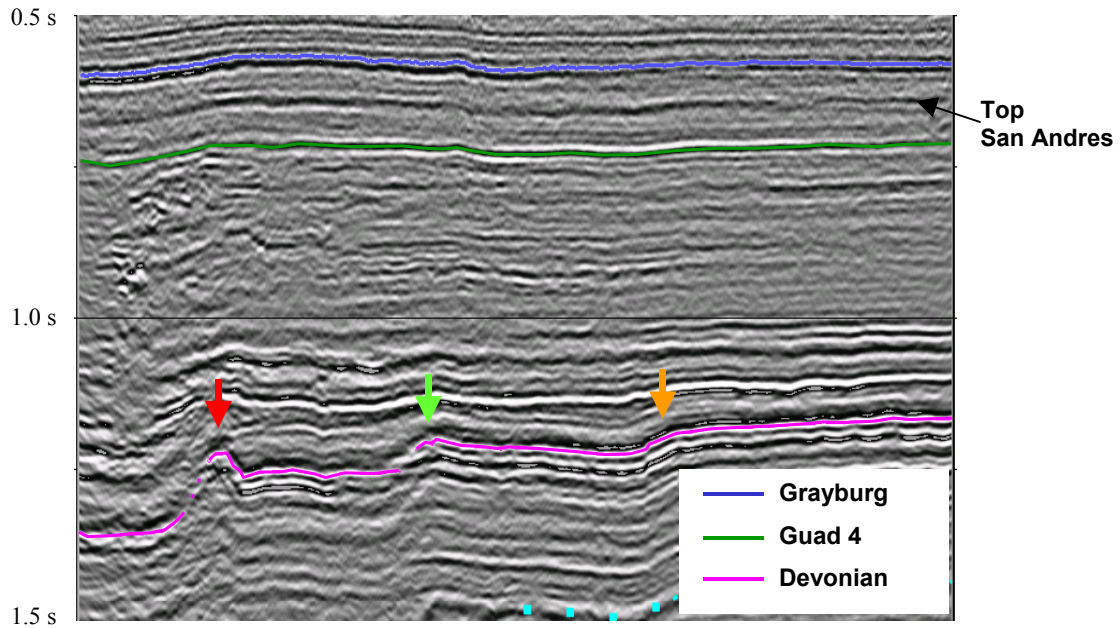


Figure 2.1.3. Top: NNE-SSW seismic section across the Waddell field 3-D seismic survey. Bottom: Most Positive curvature extraction along the pink Devonian horizon. Colored arrows highlight locations of positive curvature that can be readily identified on the vertical seismic section. These features correspond to regional faults and flexures that can be traced on the Most Positive curvature map. The blue box outlines the area shown in Figures 2.1.4 - 2.1.6.

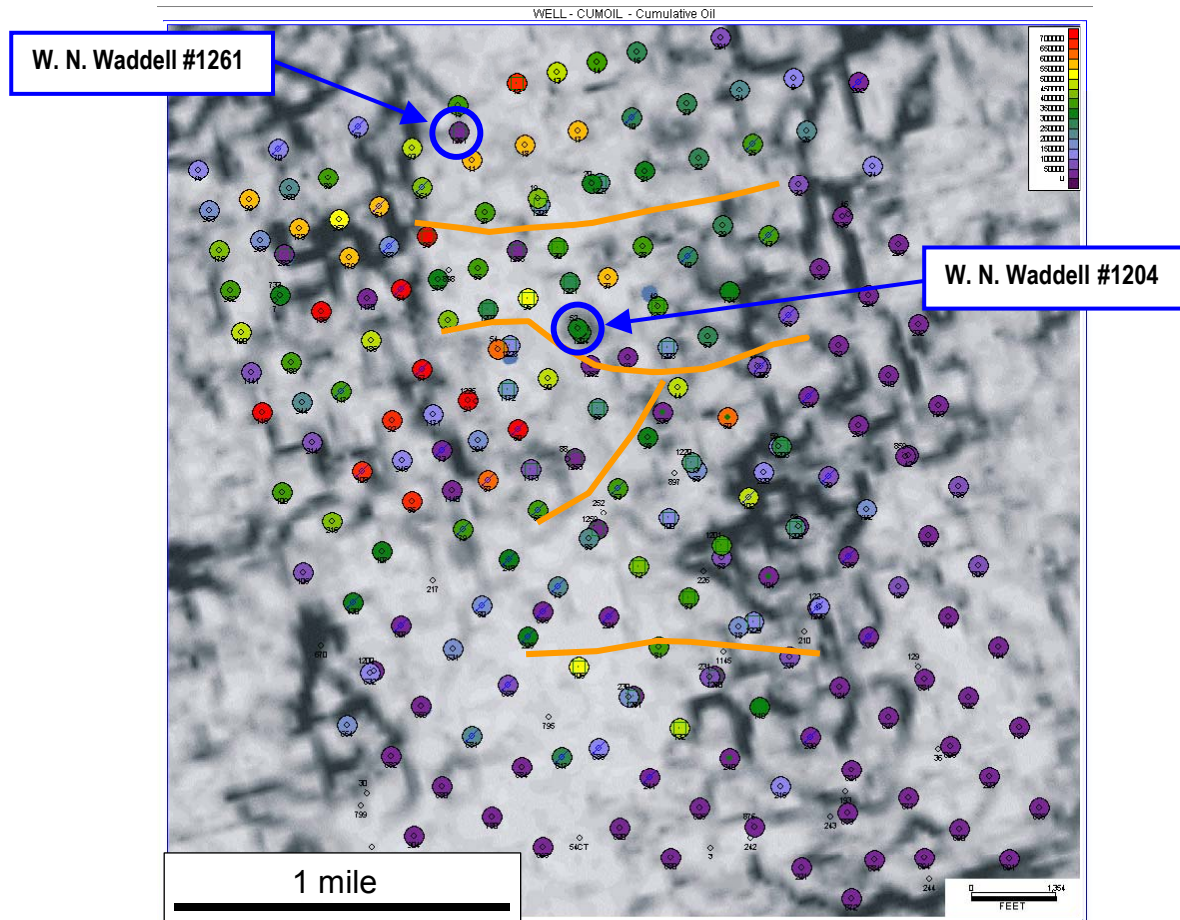


Figure 2.1.4. Coherence extraction along the top San Andres for the boxed area in Figure 2.1.3. Wells are highlighted by amount of cumulative oil production, with highest production in red. Scale is in barrels. Note that production is extremely variable but that highest production occurs primarily to the west of the high coherence (lighter gray) band in the center of the map. Engineering-based reservoir compartment boundaries are shown in orange, and do not appear to correspond to any features on the coherence map. Cored wells are denoted by the blue open circles.

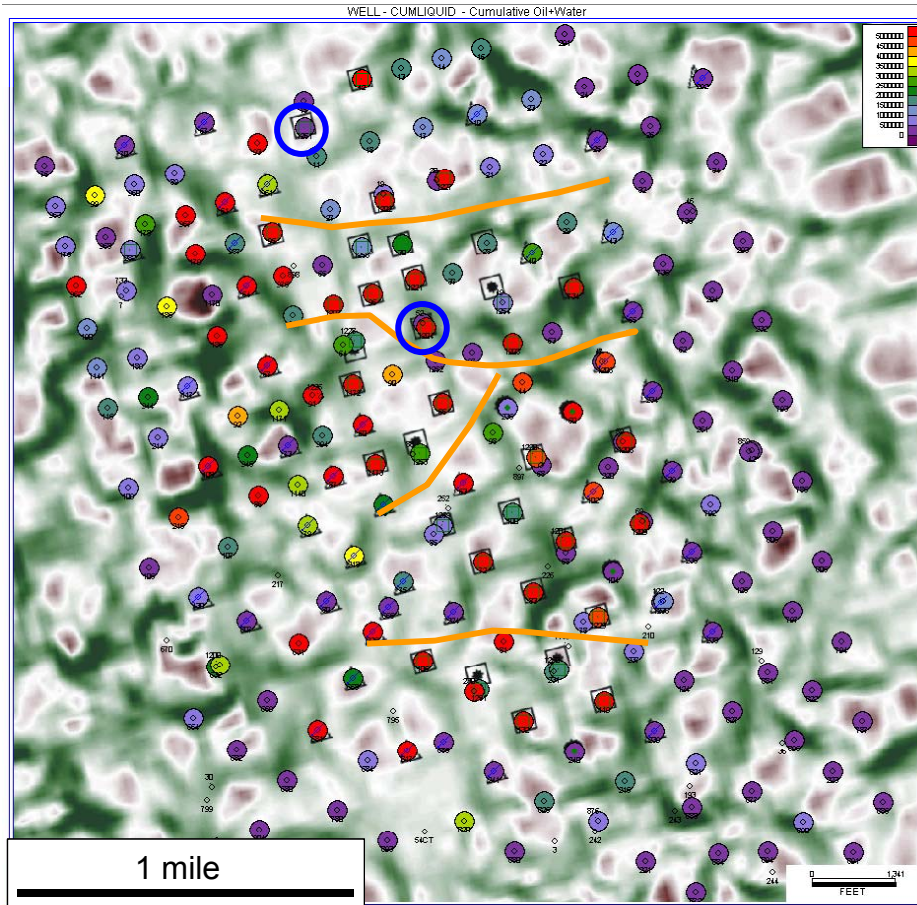


Figure 2.1.5. Most Negative curvature extraction along the top San Andres for the boxed area in Figure 2.1.3. Wells are highlighted by amount of cumulative fluid (oil + water) production, with highest production in red. Scale is in barrels. The “High Volume Area” can clearly be seen as the area with predominantly red circles. Engineering-based reservoir compartment boundaries are shown in orange and cored wells are denoted by the blue open circles. Curvature lineaments form small compartments that do not visually correlate with the engineering-based compartments.

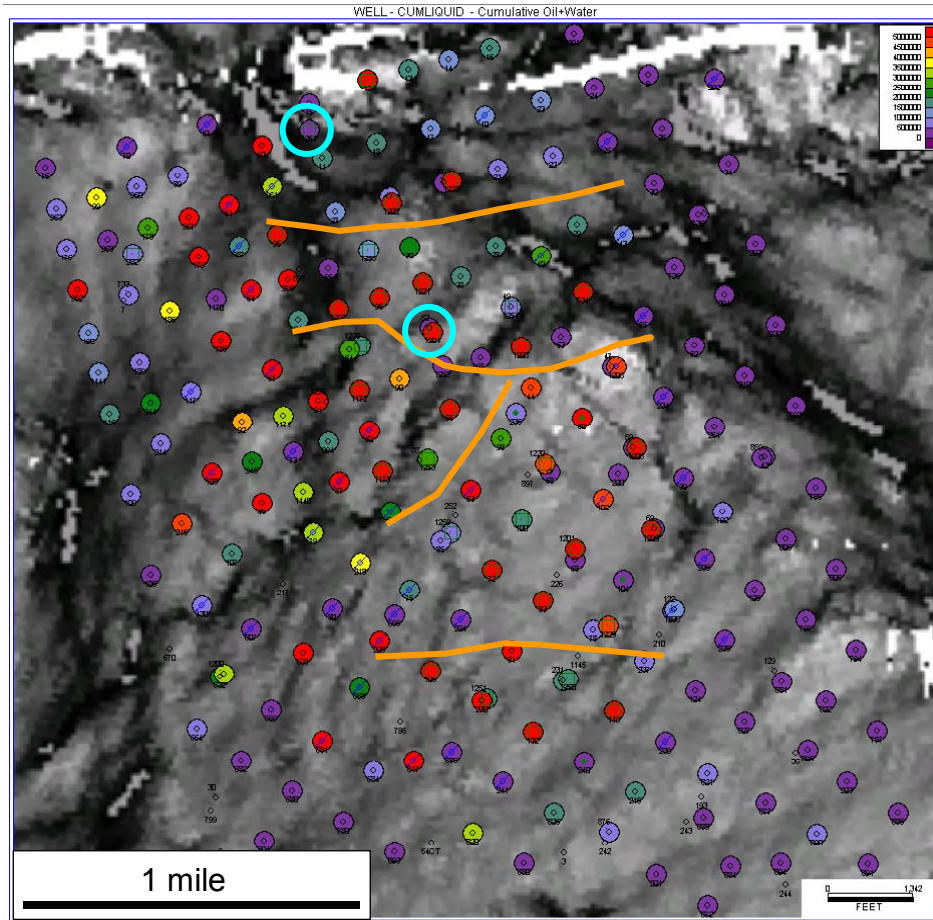


Figure 2.1.6. Most Positive curvature extraction along the Devonian horizon for the boxed area in Figure 2.1.3. Wells are highlighted by amount of cumulative fluid (oil + water) production, with highest production in red. Engineering-based reservoir compartment boundaries are shown in orange and cored wells are denoted by the blue open circles. Note that the engineering-based compartment boundaries appear to coincide with truncations or offsets in some of the curvature lineaments.

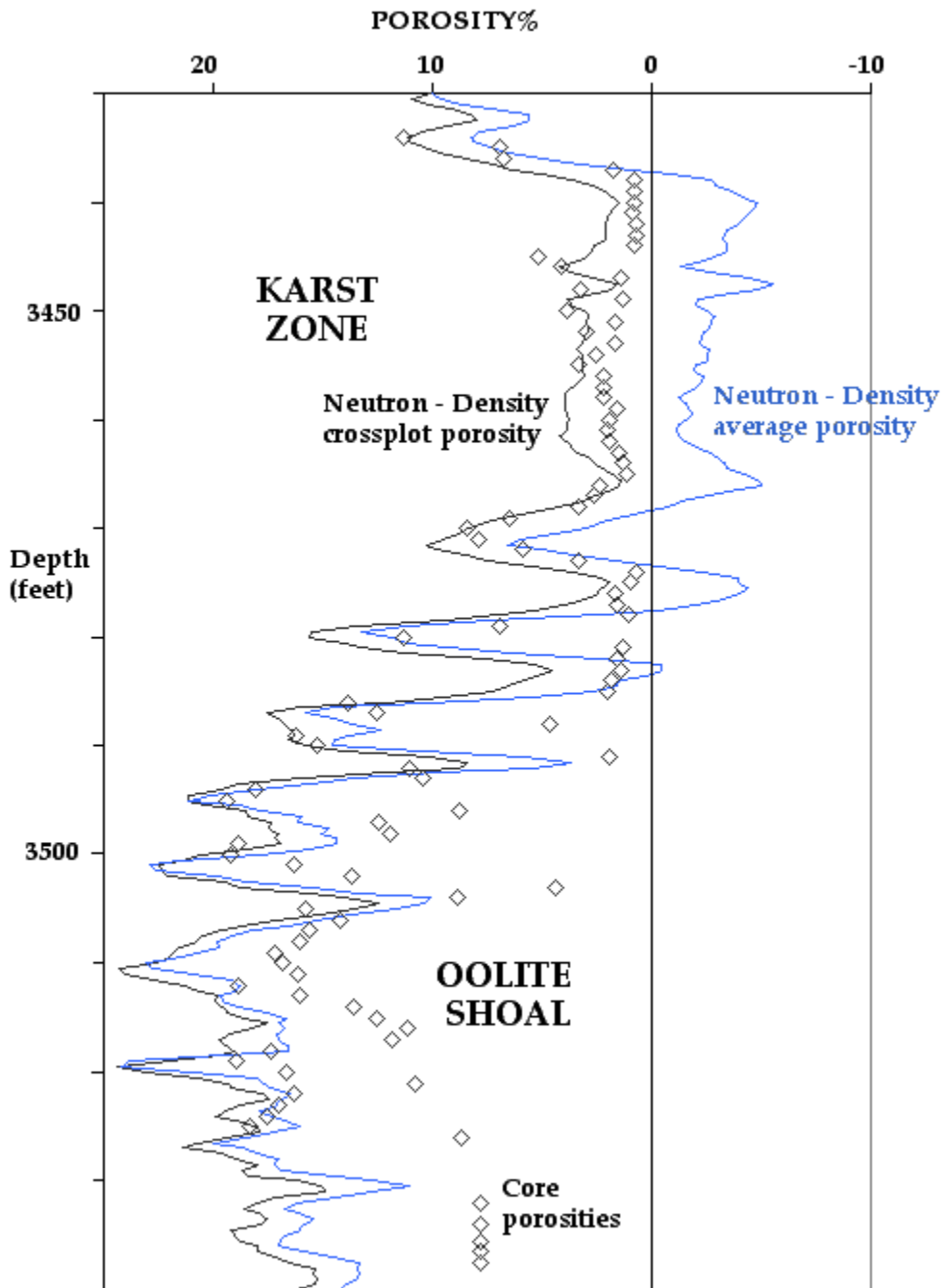


Figure 2.1.7. Neutron-density log porosities versus core porosity in the cored interval of the San Andres Formation in W. N. Waddell #1261.

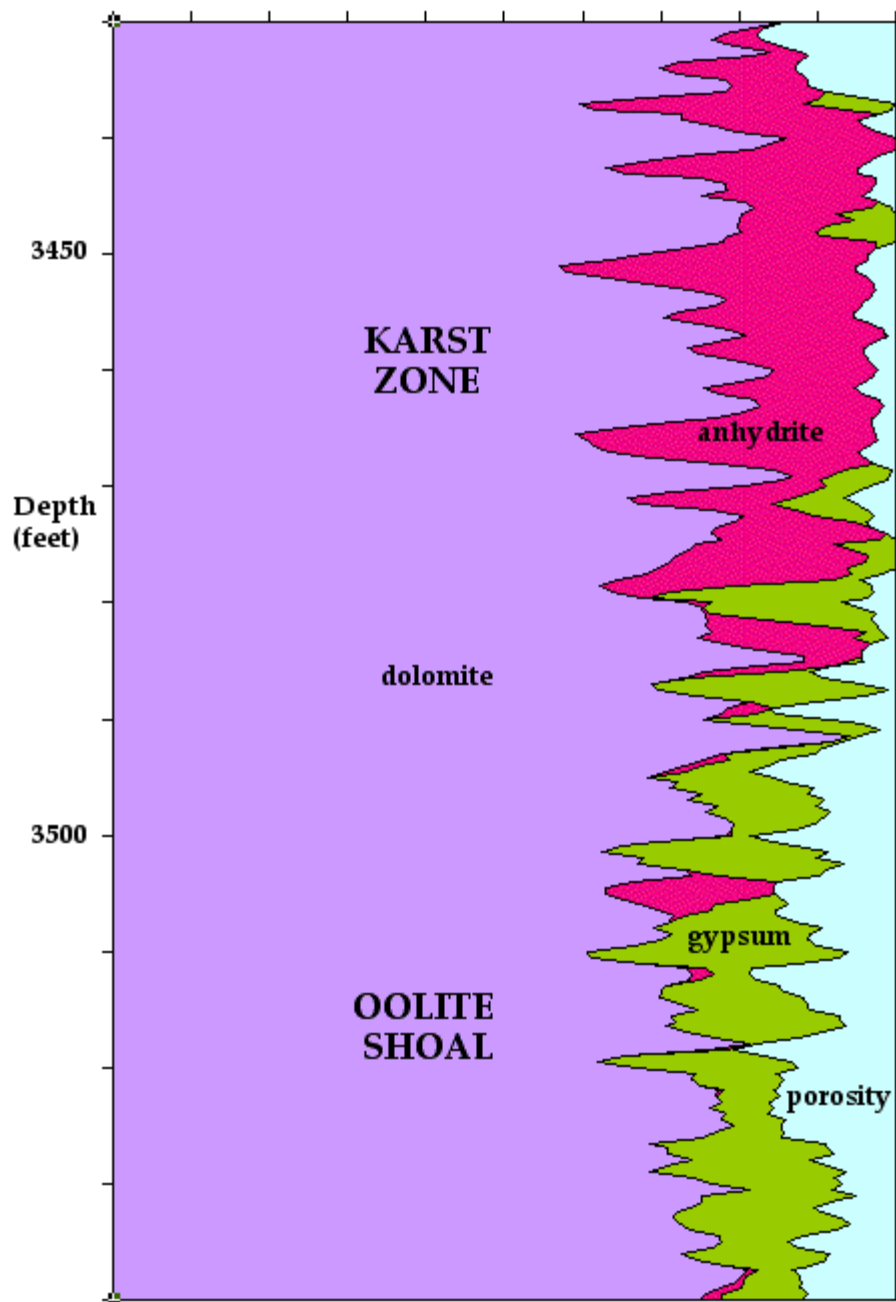


Figure 2.1.8. Compositional analysis of minerals and pore volume in the cored interval of the San Andres Formation in W. N. Waddell #1261 based on neutron, density, and photoelectric factor logs.

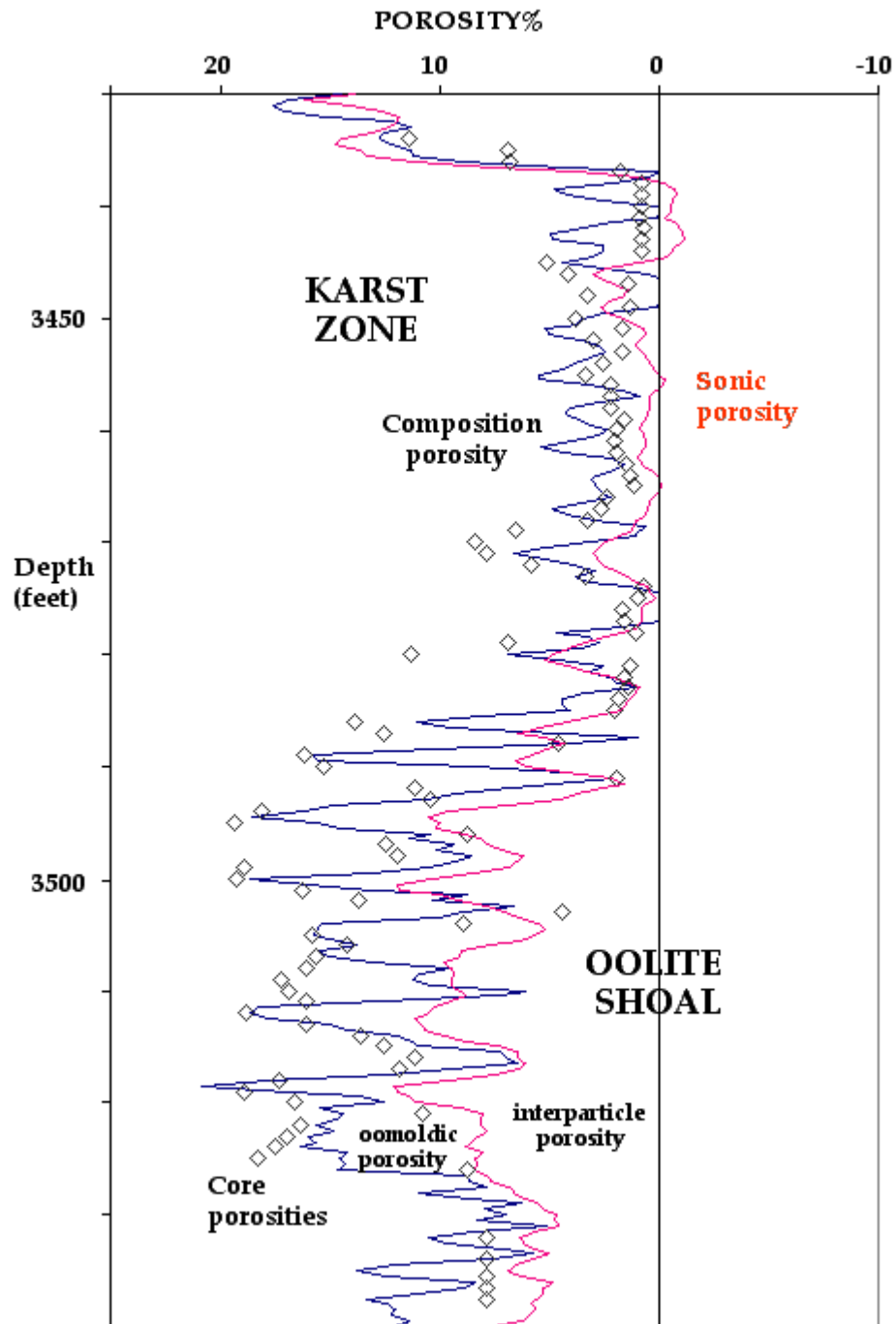


Figure 2.1.9. Compositional pore volume and sonic log porosity versus core porosity in the cored interval of the San Andres Formation in W. N. Waddell #1261.

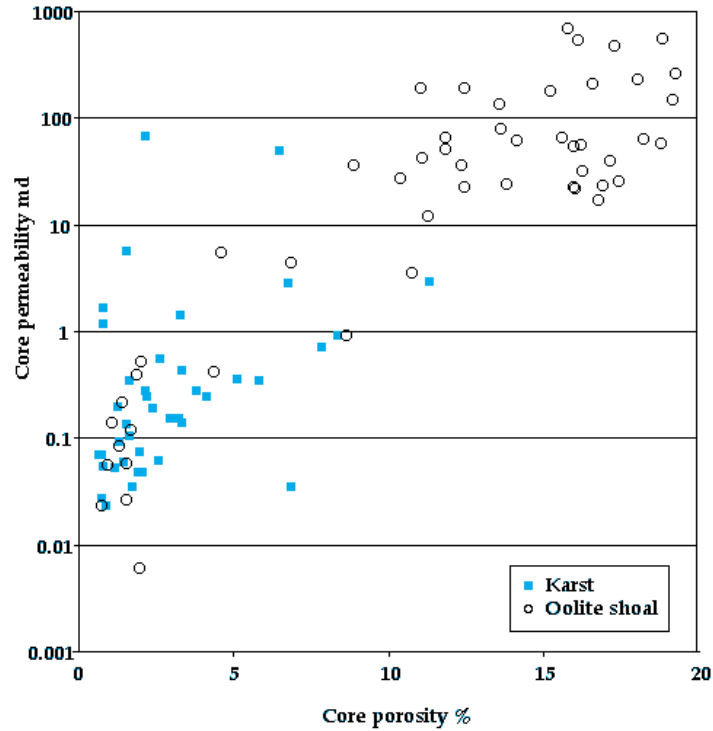


Figure 2.1.10. Core porosity and permeability crossplot of the San Andres Formation in W. N. Waddell #1261.

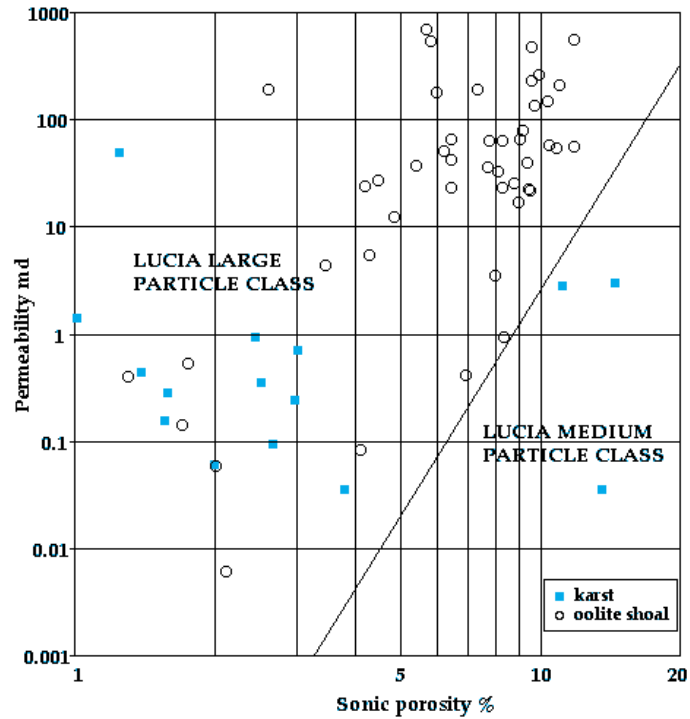


Figure 2.1.11. Sonic porosity and core permeability crossplot of the San Andres Formation in W. N. Waddell #1261.

Era	System	Series	Stratigraphic Unit
Paleozoic	Pennsylvanian	Virgilian	Wabunsee Group
			Shawnee Group
			Douglas Group
		Missourian	Lansing Group
			Kansas City Group
			Pleasanton Group
		Desmoinesian	Marmaton Group
			Cherokee Group
		Atokan	
	Mississippian	Morrowan	Keyes Formation
			St. Louis Ls.
			Salem (Spergen) Ls.
		Meramecian	Warsaw Ls.
Osagian			
Kinderhookian			

Figure 2.2.1. Stratigraphic column for Mississippian study area, Cheyenne County, Colorado. Spergen reservoir interval is highlighted in green.

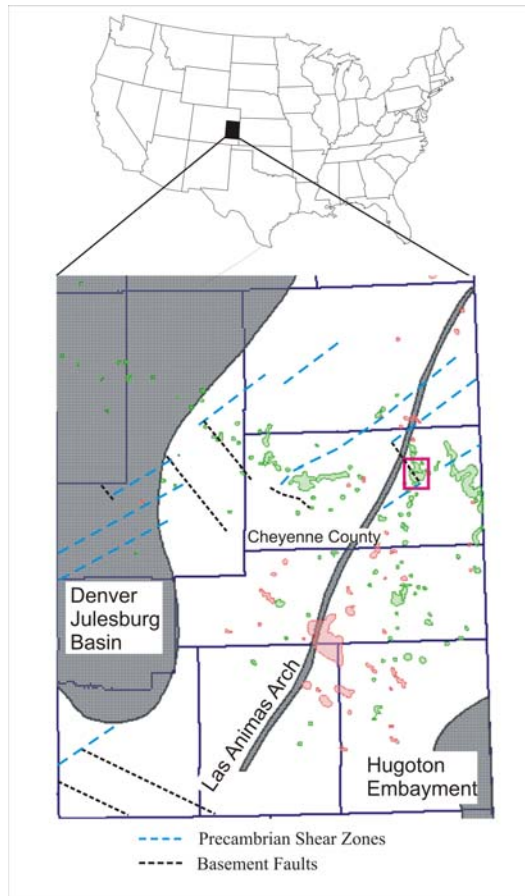


Figure 2.2.2. Map of major structural features of eastern Colorado showing oil (green) and gas (red) fields. The pink box outlines the location of the study area. Map modified from Sims et al. (2001) and <http://oil-gas.state.co.us/infosys/maps>.

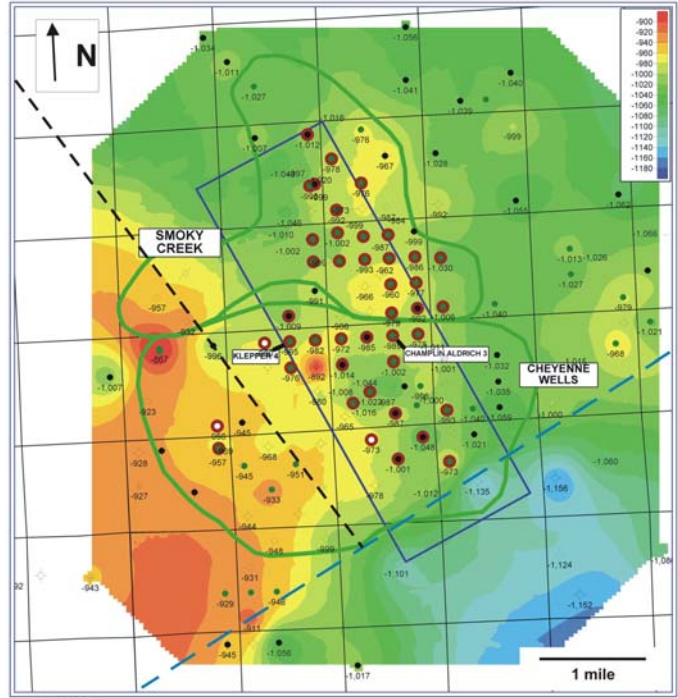


Figure 2.2.3. Structure map of the top of the Pennsylvanian Keys Formation in the area outlined by the pink box in Figure 2.2.2. Top Keys subsea depths in feet are labeled at the well locations. Field outlines are shown in green. 3-D seismic survey is outlined in blue. Wells with Spergen production are highlighted in red. Cored wells are labeled. Locations of a high angle basement fault (dashed black line) and Precambrian shear zone (dashed blue line) from Sims et al. (2001) are shown.

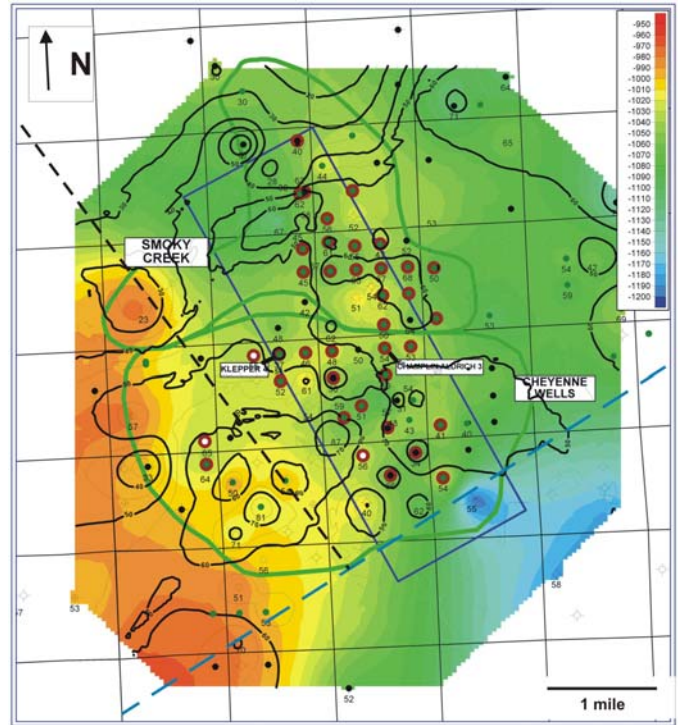


Figure 2.2.4. Structure map on top of the St. Louis (color filled contours) with isopach of the interval between the top of the Keys Formation and the top of the St. Louis superimposed (black, 5 ft. contour interval). Isopach thicknesses in feet are labeled at wells. Other elements as in Figure 2.2.3.

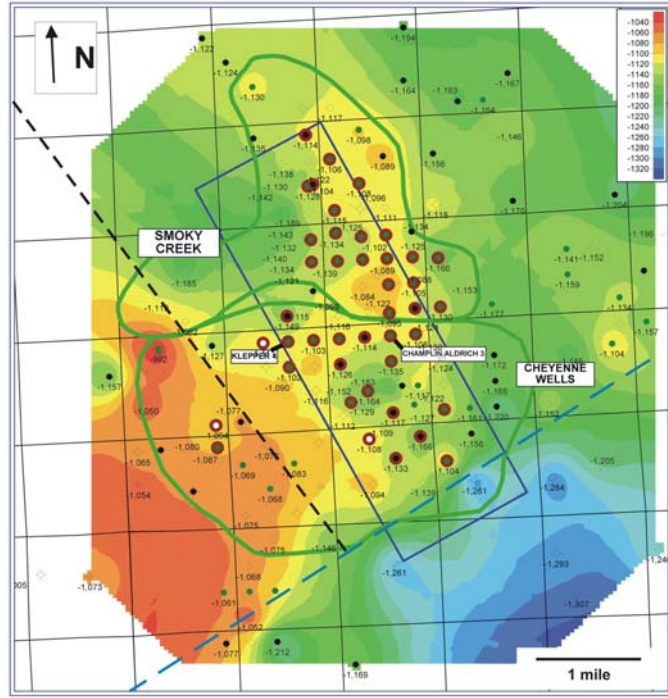


Figure 2.2.5. Structure map on top of the Spergen. Top Spergen subsea depths in feet are labeled at the well locations. Other map elements as in Figure 2.2.3.

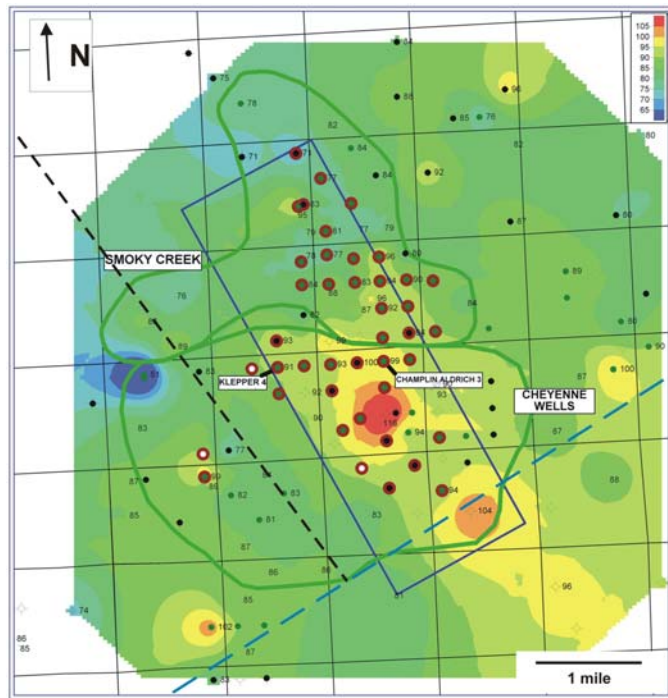


Figure 2.2.6. Isopach of gross Spergen thickness. Isopach thicknesses in feet are labeled at wells. Other map elements as in Figure 2.2.3.

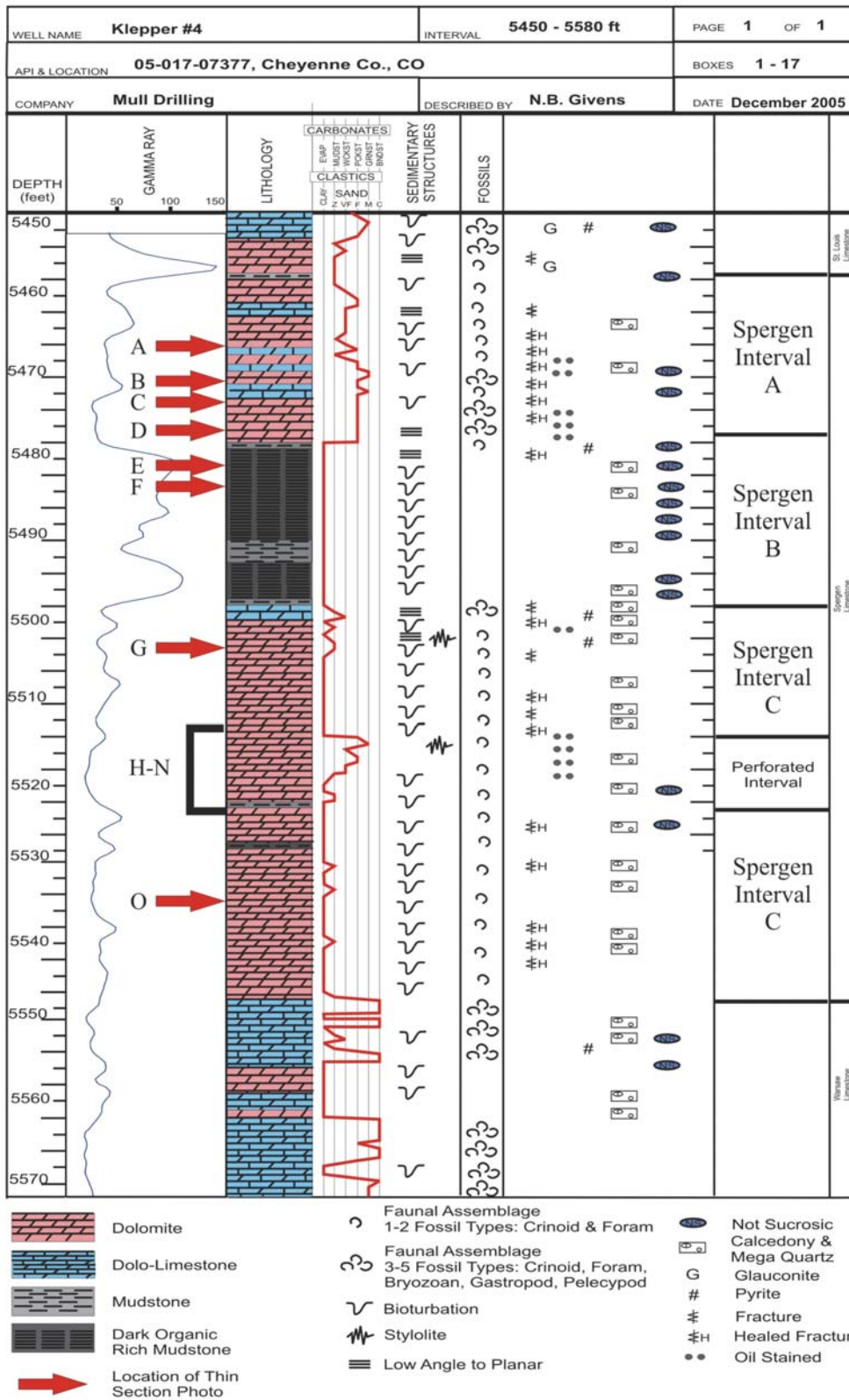


Figure 2.2.7. Core description of Klepper #4. Locations of thin section photos A-O in Figure 2.2.9 are shown by red arrows.

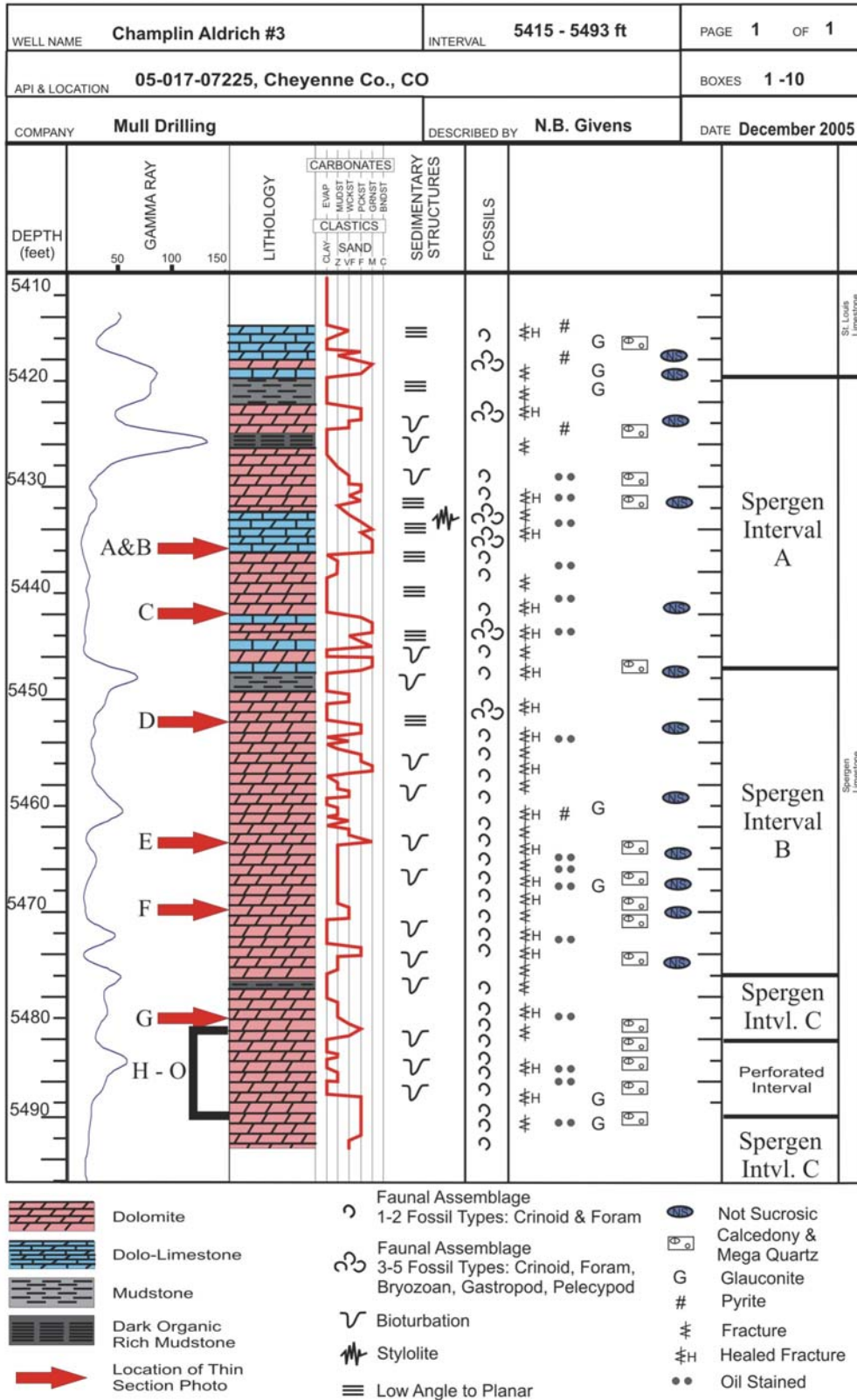


Figure 2.2.8. Core description of Champlin Aldrich #3. Locations of thin section photos A-O in Figure 2.2.10 are shown by red arrows.

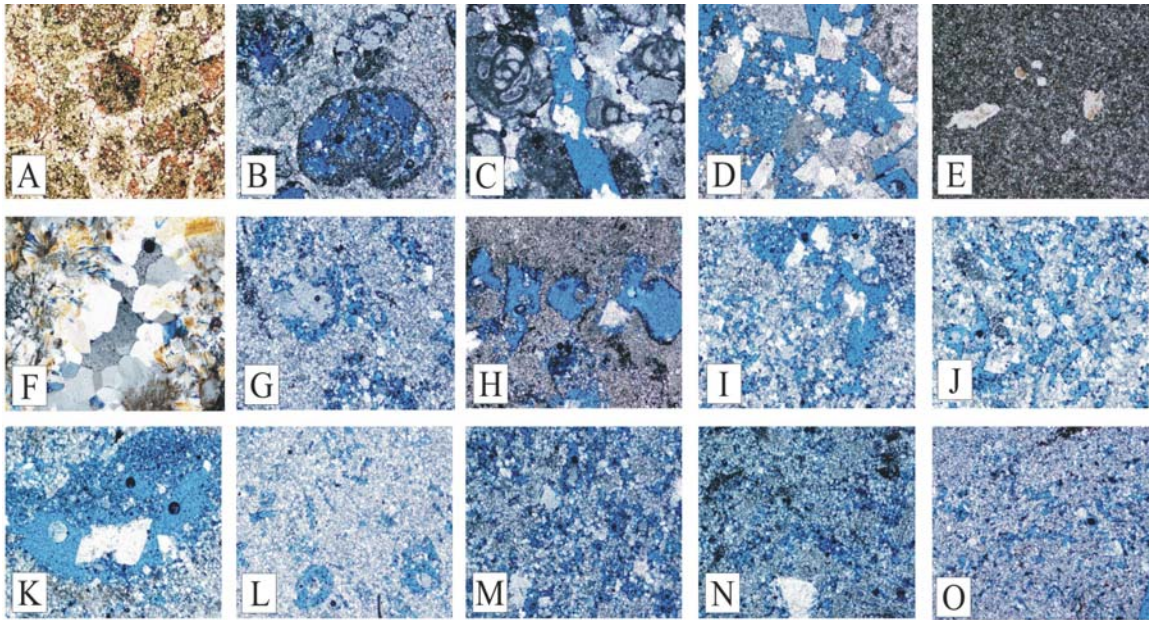


Figure 2.2.9. Thin section photomicrograph images from Klepper #4. Images H-N are from the perforated interval. A) (5466.5) Stained slide showing calcite (pink) fossil fragments and cement, dolomite (colorless), no visible solution-enhanced porosity (4x). B) (5470.5) Foram moldic porosity (4x). C) (5472.7) Baroque dolomite in fracture in a foram grainstone (crossed Nicols) (4x). D) (5477.5) Large solution-enhanced porosity with baroque dolomite (4x). E) (5480.4) Calcedony crystals in an organic-rich mudstone (4x). F) (5481.2) Calcedony (brown), megaquartz (colorless) and baroque dolomite (colorless-center) solution-enhanced void fill (crossed Nicols) (4x). G) (5502.7) Fine to medium crystalline dolomite with baroque dolomite filling solution-enhanced porosity (4x). H) (5514.2) Very fine crystalline dolomite and solution-enhanced porosity (4x). I) (5415.4) Fine to medium crystalline dolomite and baroque dolomite filling solution-enhanced porosity (crossed Nicols) (4x). J) (5416.5) Medium crystalline dolomite and baroque dolomite filling solution-enhanced porosity (crossed Nicols) (4x). K) (5418.8) Large solution-enhanced porosity with baroque dolomite fill (crossed Nicols) (4x). L) (5419.6) Moldic and solution-enhanced porosity in a finely crystalline dolomite (crossed Nicols) (4x). M) (5420.7) Solution-enhanced porosity and baroque dolomite fill (crossed Nicols) (4x). N) (5422.7) Solution-enhanced porosity (crossed Nicols) (4x). O) (5534.5) Smaller solution-enhanced porosity in a fine crystalline dolomite (4x).

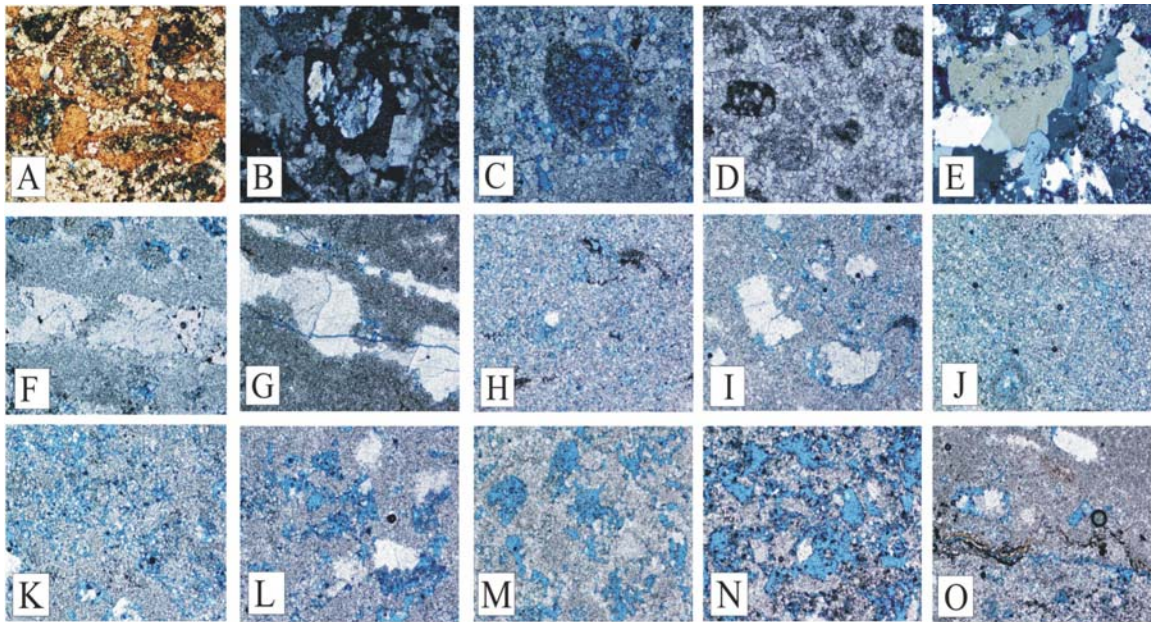


Figure 2.2.10. Thin section photomicrograph images from Champlin Aldrich #3. Images H-O are from the perforated interval. A) (5435.2') Stained slide showing calcite (pink) fossil fragments, cement, dolomite (colorless) and solution-enhanced porosity (blue) (4x). B) (5435.2') Silica replacement of crinoid fragment (crossed polars) (4x). C) (5441.3') Very fine to medium crystalline dolomite with foram moldic and solution-enhanced porosity (4x). D) (5451.2') Foram-rich wackepackstone with no visible solution-enhanced porosity (4x). E) (5463.7') Megaquartz solution-enhanced void fill and fine crystalline dolomite (crossed Nicols) (4x). F) (5469.5') Baroque dolomite replacement (4x). G) (5479.9') Baroque dolomite fill of solution-enhanced fracture (4x). H) (5482.4') Area of higher percentage of solution-enhanced porosity within a mudstone (4x). I) (5484.5') Baroque dolomite filling solution-enhanced porosity (4x). J) (5485.5') Very fine crystalline dolomite with small solution-enhanced porosity (4x). K) (5486.2') Baroque dolomite filling solution-enhanced porosity (4x). L) (5486.4') Large solution-enhanced and possibly moldic porosity filled by baroque dolomite (4x). M) (5487.2') Large solution-enhanced and moldic porosity, less baroque dolomite (4x). N) (5487.8') Large solution-enhanced and moldic porosity and some baroque dolomite (4x). O) (5488.3') Less solution-enhanced porosity with baroque dolomite fill (4x).

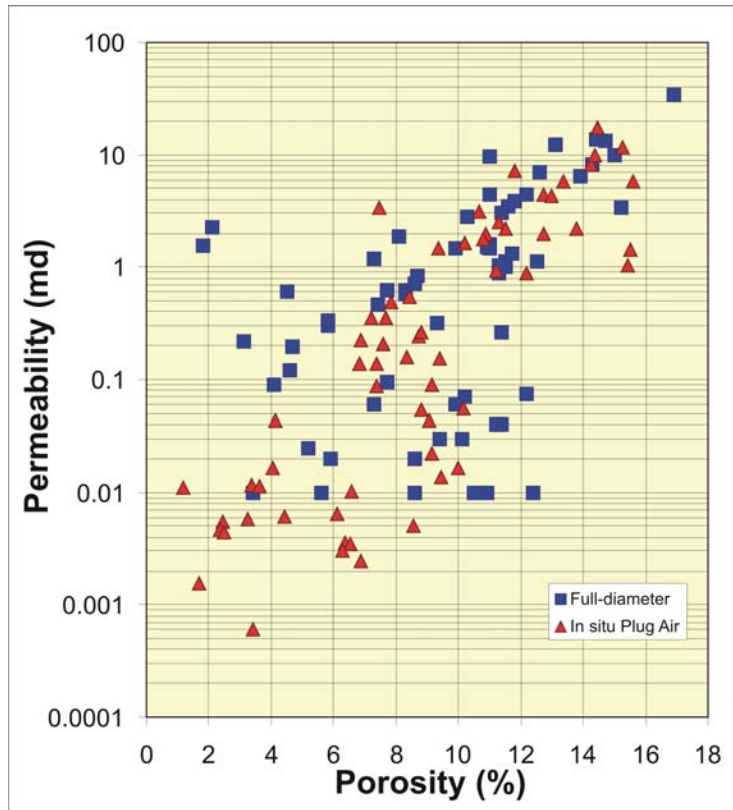


Figure 2.2.11. Graph of permeability versus porosity for plug and full-diameter samples from Champlin-Aldrich #3.

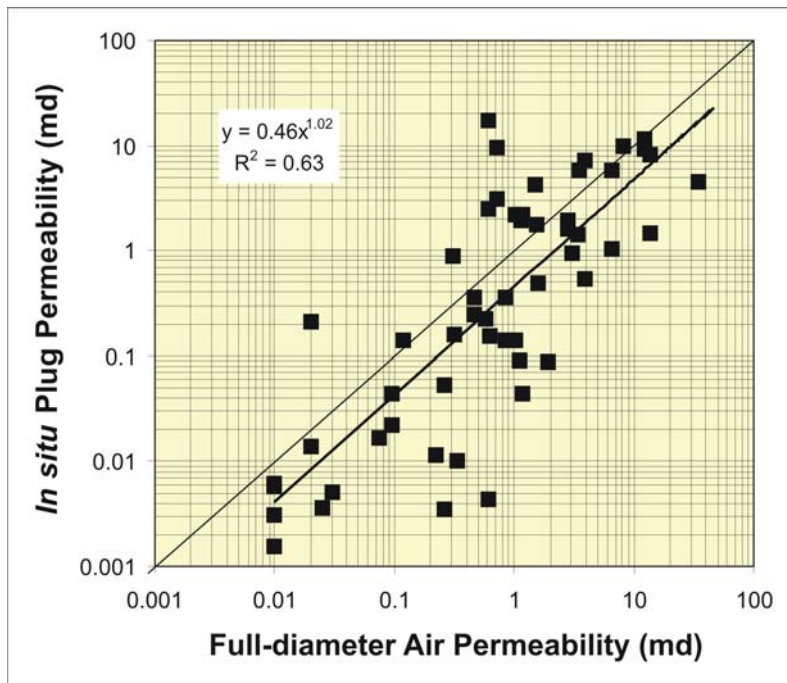


Figure 2.2.12. Graph of *in situ* plug permeability versus full-diameter air permeability. Differences reflect effects of confining stress difference.

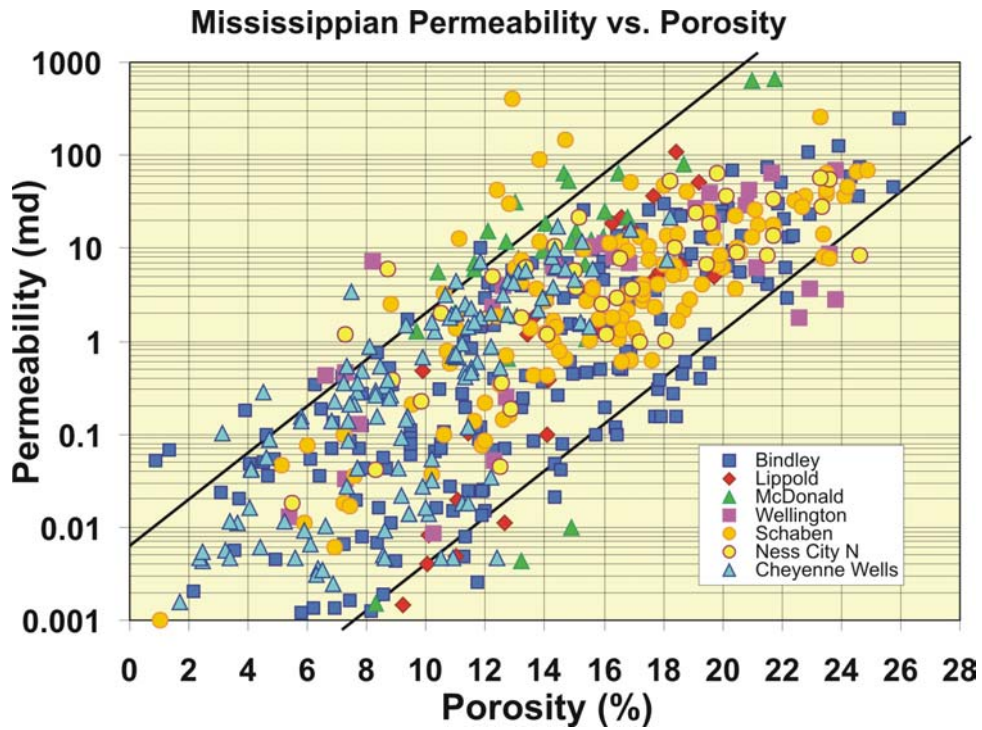


Figure 2.2.13. Graph of permeability versus porosity for all lithofacies for the two cores from Cheyenne Wells field, along with data from six Mississippian fields in Kansas (Bhattacharya et al., 2005). Bounding trend lines are shown in black.

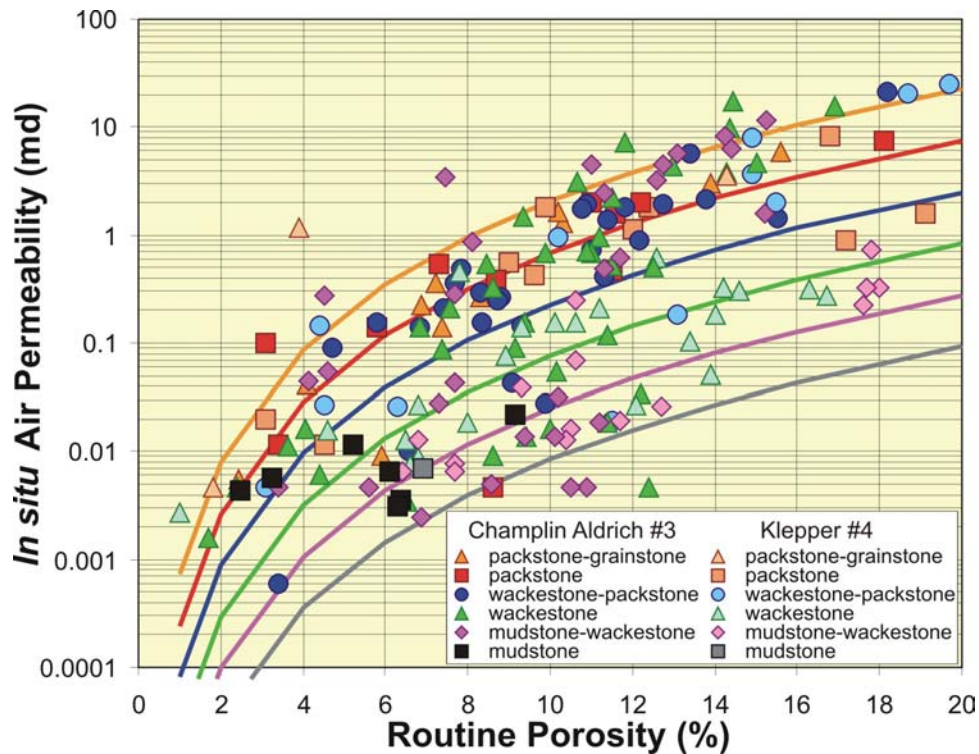


Figure 2.2.14. Graph of permeability versus porosity for different lithofacies from Champlin Aldrich #3 and Klepper #4. A trend line is shown for each lithofacies. Equations for the trend lines are presented in the text.

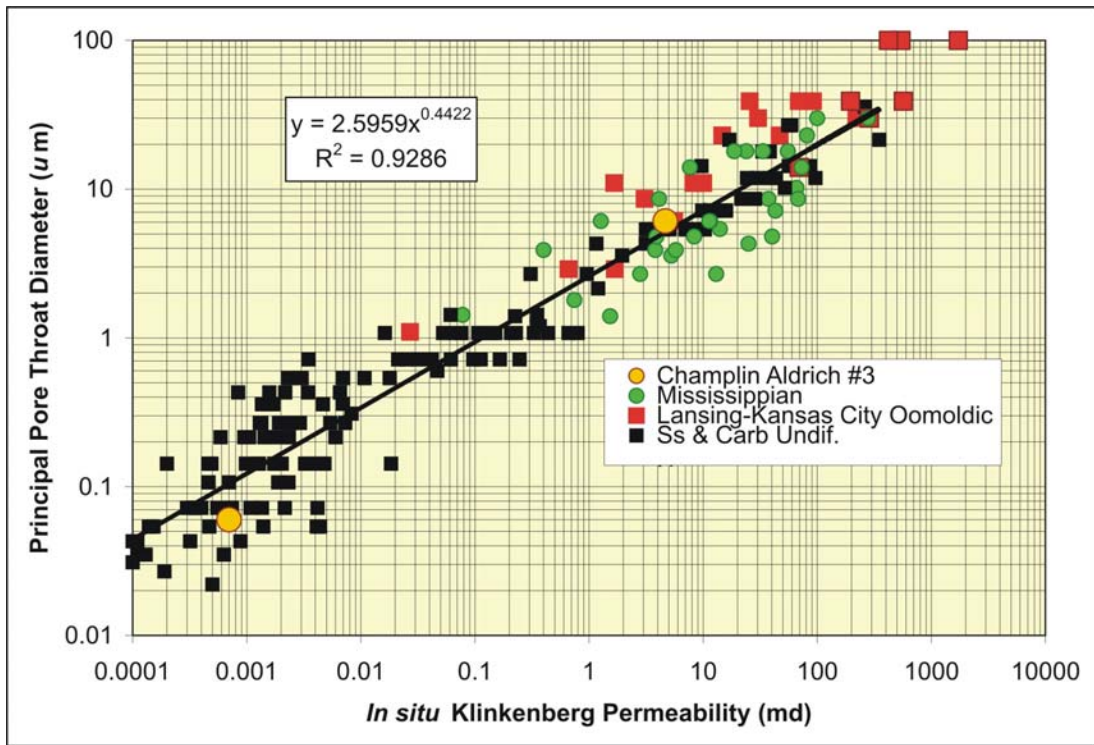


Figure 2.2.15. Crossplot of principal pore throat diameter versus permeability for two samples from Champlin Aldrich #3 (yellow) compared to undifferentiated sandstones and carbonates (black), and differentiated Lansing-Kansas City (red) and Mississippian (green) moldic carbonates from Byrnes et al. (2003).

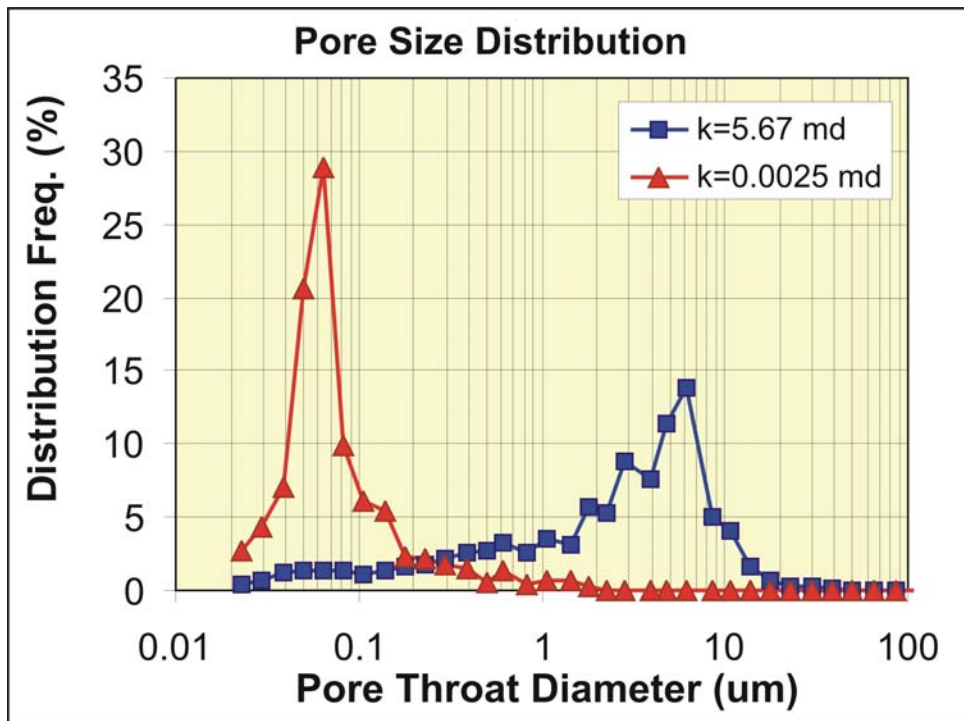


Figure 2.2.16. Pore throat size distributions for a low permeability mudstone-wackestone (red) and a higher permeability packstone (blue). Both rocks show unimodal distribution.

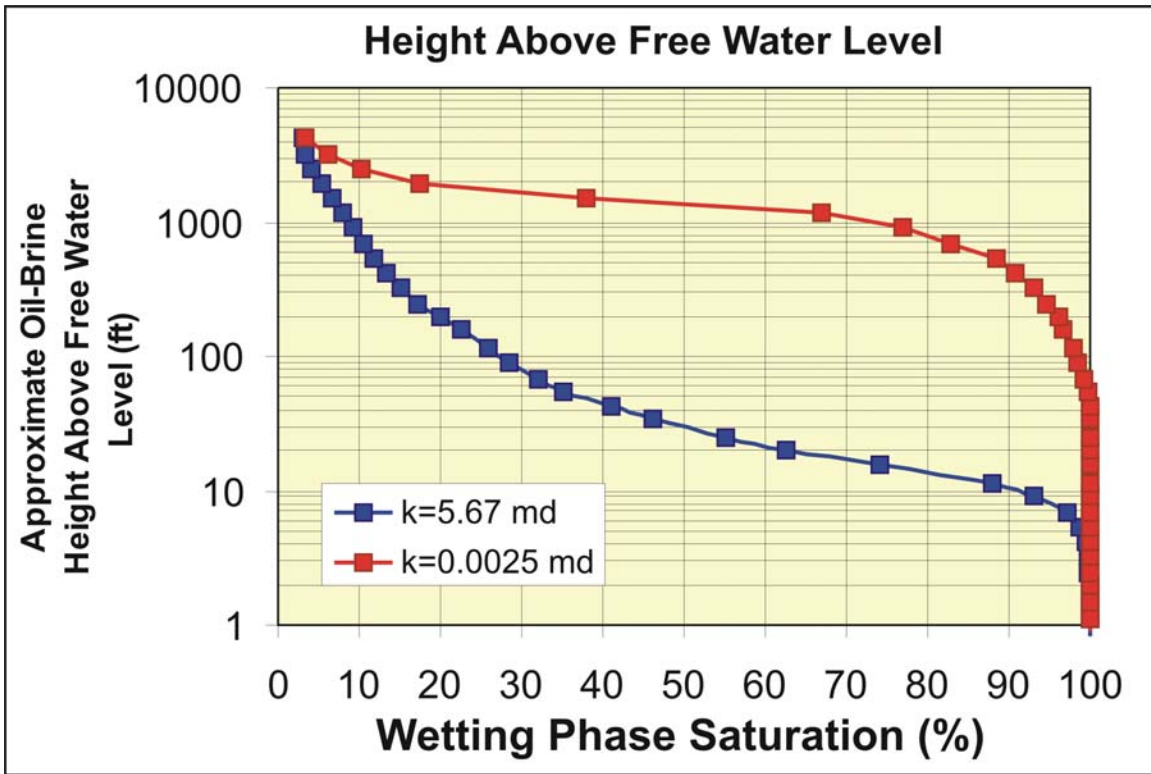


Figure 2.2.17. Capillary pressure curves for a low permeability mudstone-wackestone (red) and a higher permeability packstone (blue) illustrating upper and lower limits for rocks from the Cheyenne Wells field.

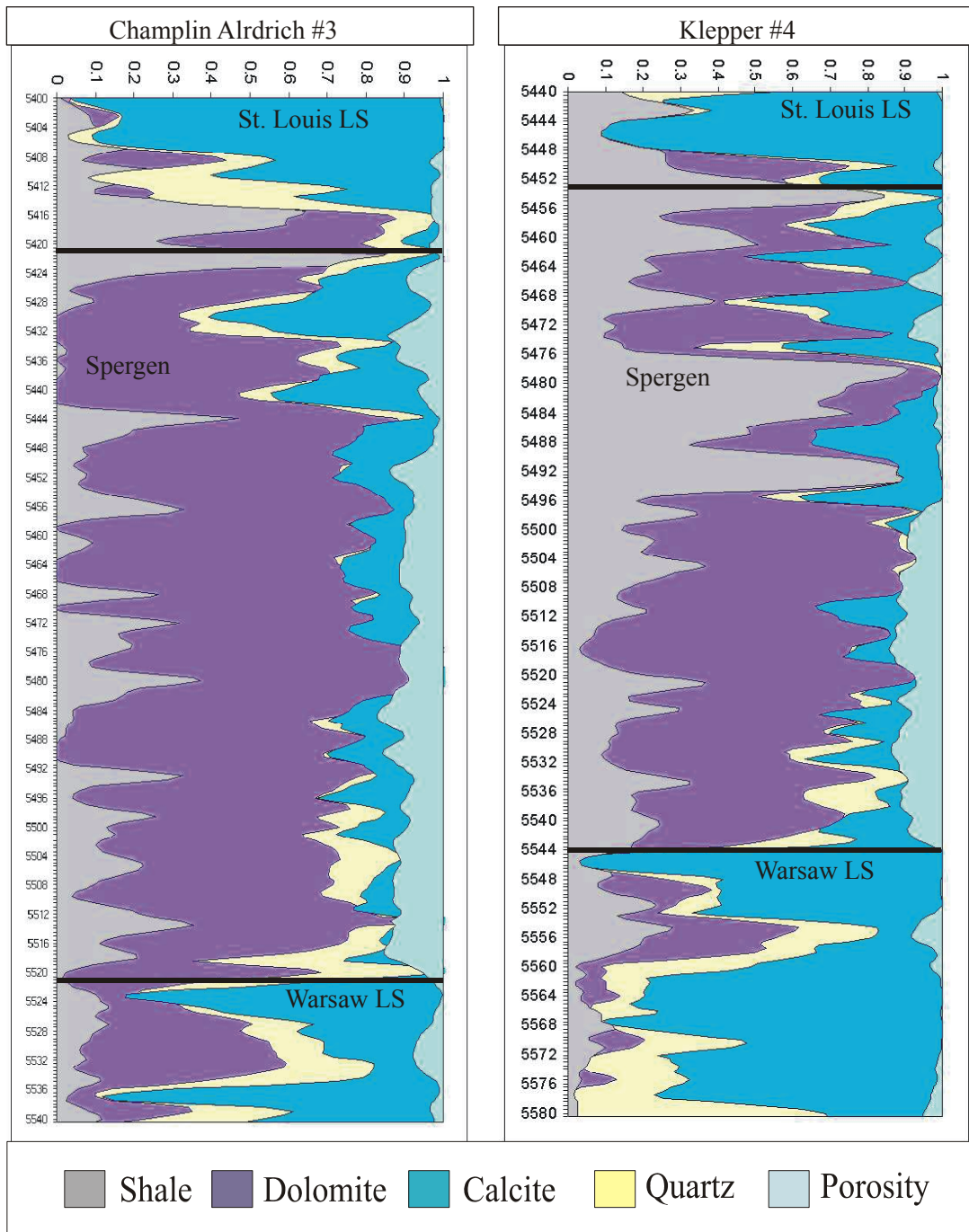
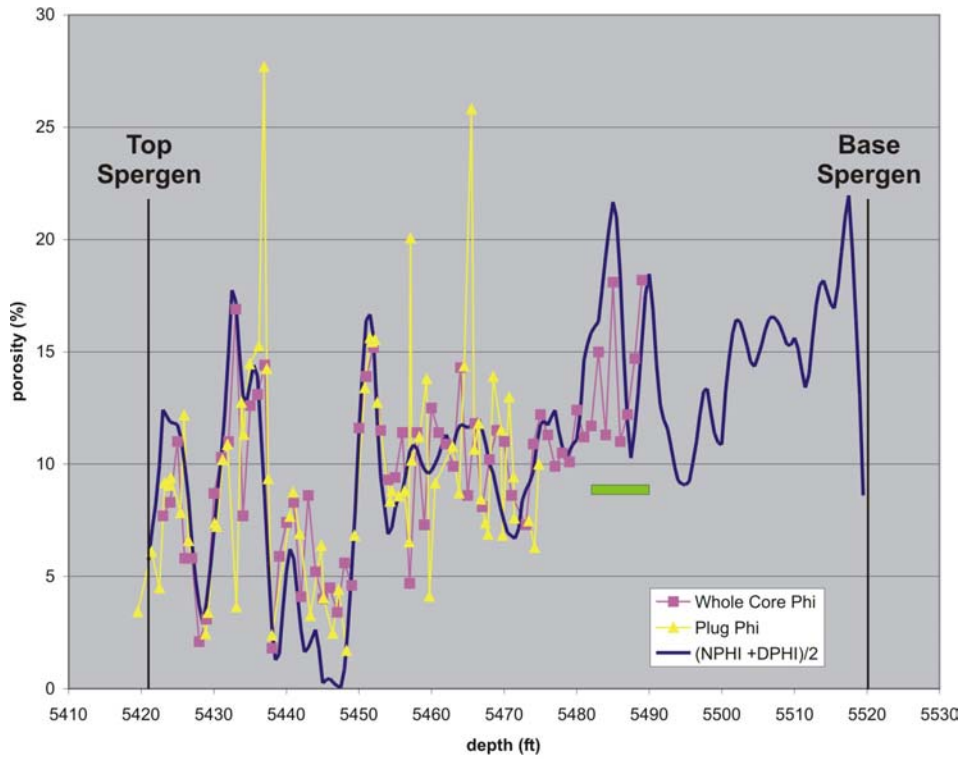


Figure 2.2.18. Composition graphs for Champlin Aldrich #3 (left) and Klepper #4 (right) created from wireline log data using a matrix algebra solution in Excel. Mineral compositions estimated from the logs show good concordance with lithologies described from core.

Champlin Aldrich #3



Klepper #4

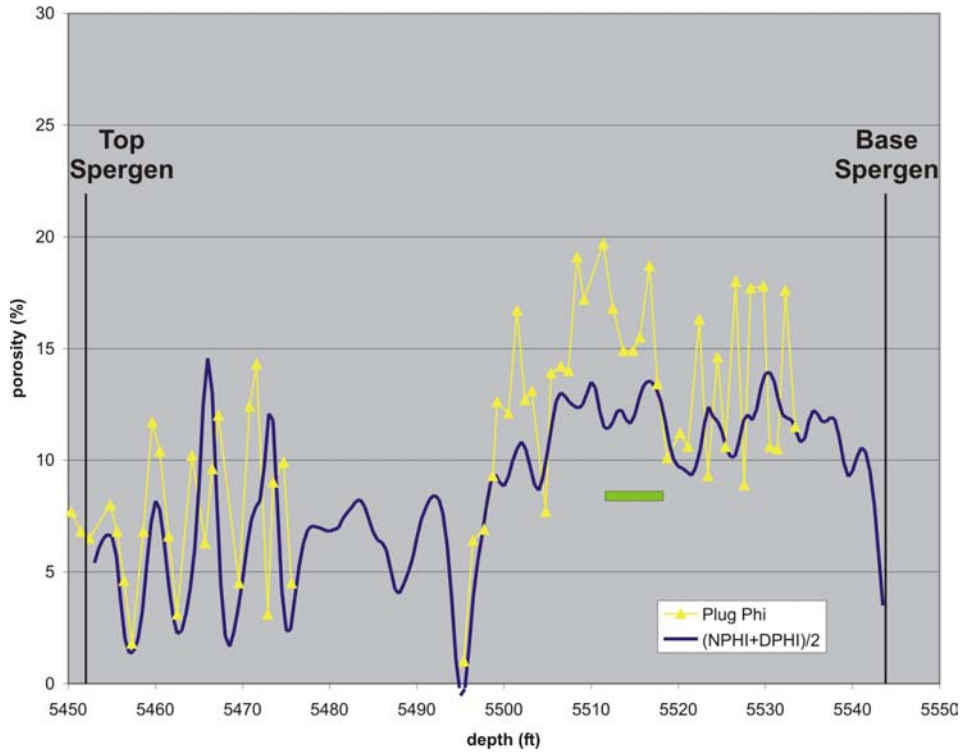


Figure 2.2.19. Graph of average neutron-density log porosity (blue) and core helium porosity (purple – whole core; yellow - plug) versus depth in Champlin Aldrich #3 (top) and Klepper #4 (bottom). The perforated intervals are indicated by the green lines.

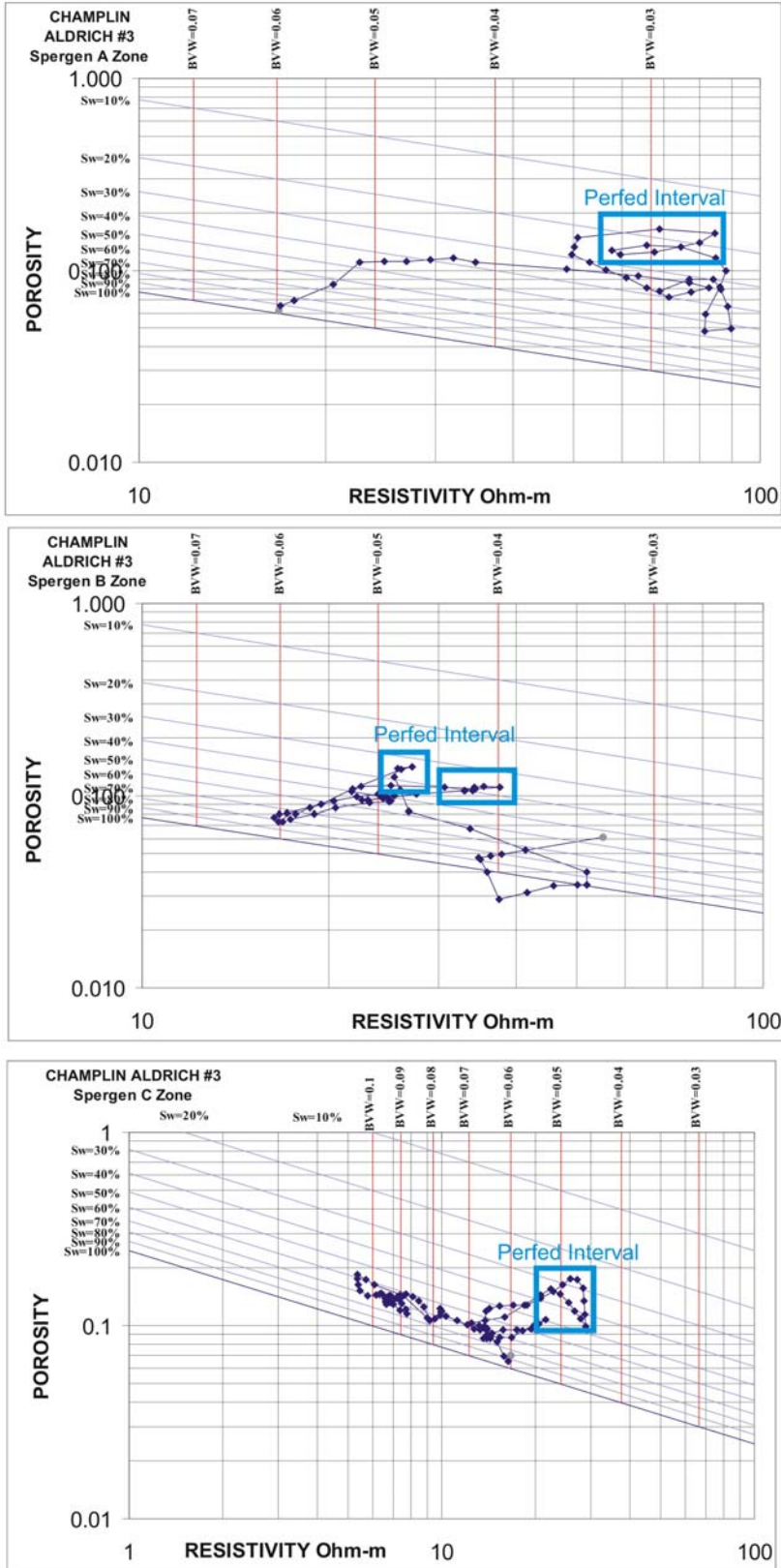


Figure 2.2.20. Pickett plots for Spergen A, B, and C zones in Champlin-Aldrich #3. The perforated intervals are indicated by blue boxes.

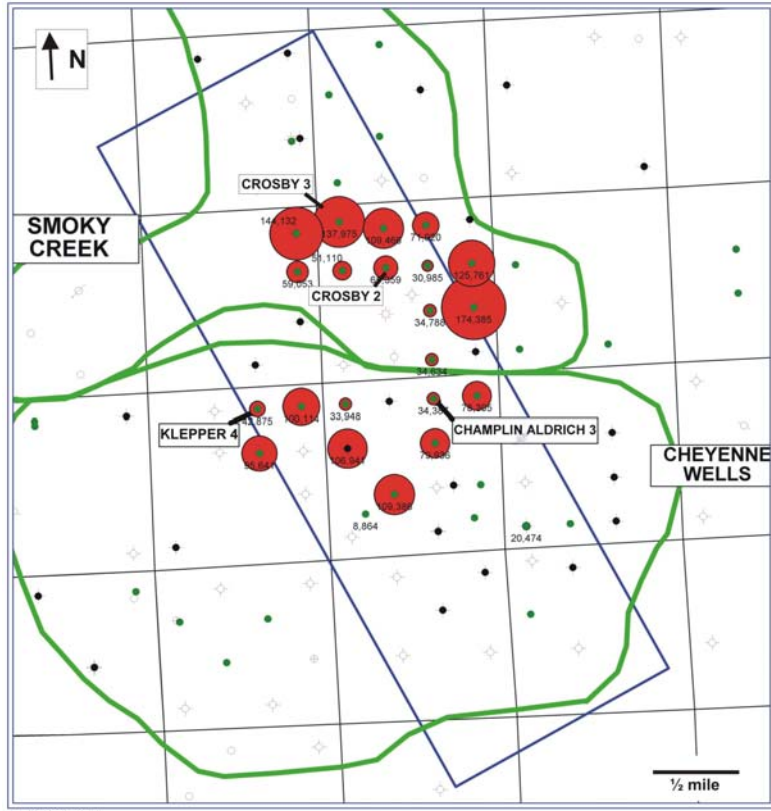


Figure 2.2.21. Bubble map showing with red circles the relative amount of oil produced from the Spergen during the first 60 months of production for each well. The largest circle corresponds to 174,385 barrels. Wells discussed in the text are labeled.

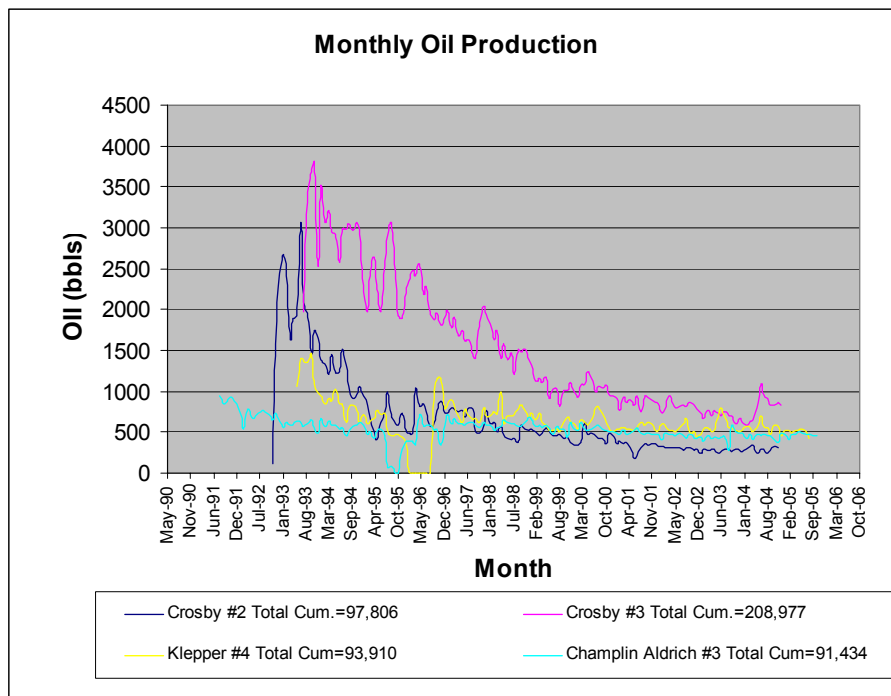


Figure 2.2.22. Comparison of production profiles for four Spergen wells in the Cheyenne Wells and Smoky Creek fields.

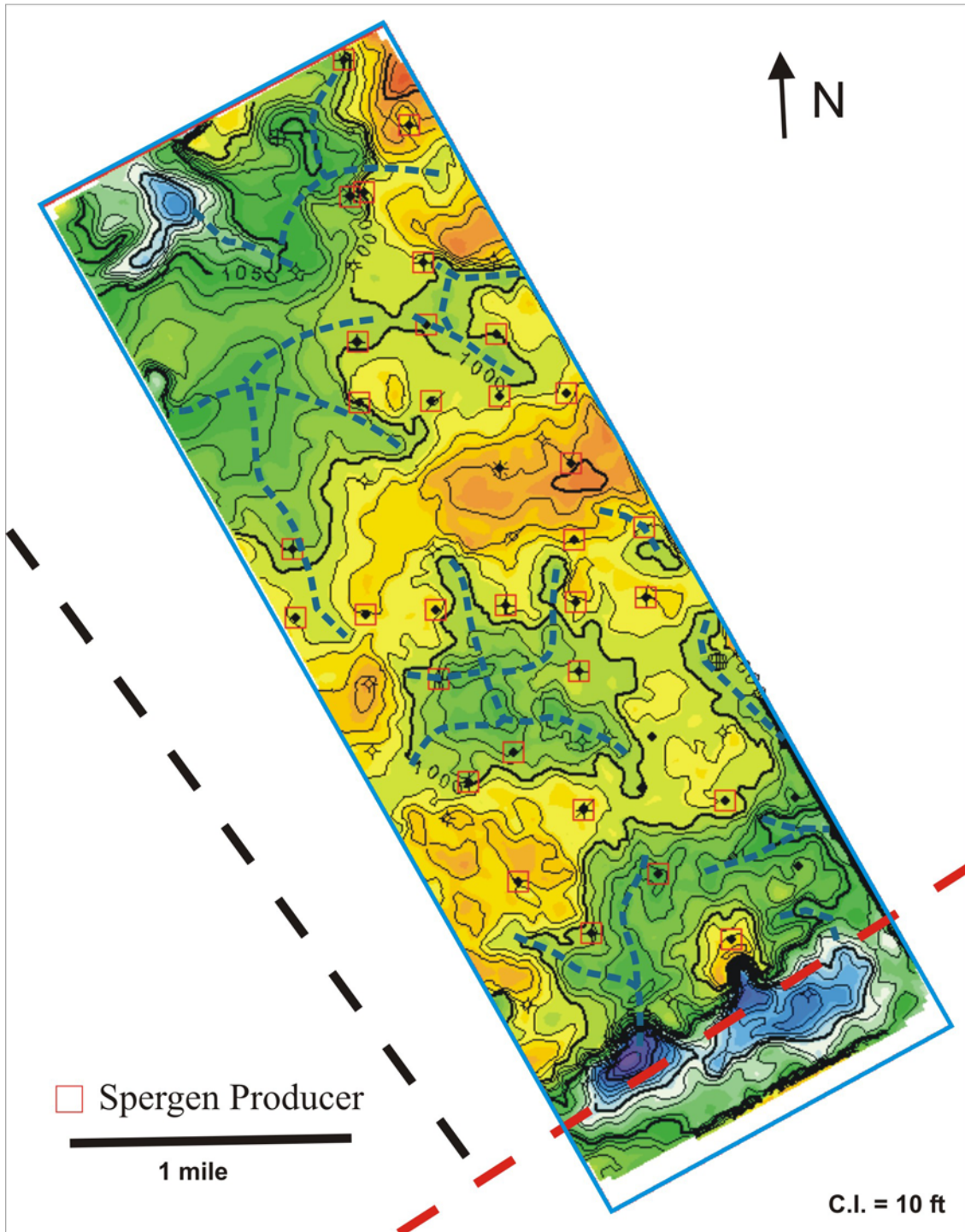


Figure 2.2.23. Top Keys subsea depth structure map derived from seismic data. Orange indicates structural highs and purple indicates structural lows. Interpreted drainage patterns are indicated by blue dashed lines. The red dashed line is a Precambrian shear zone and the black dashed line is a high angle basement fault from Sims et al. (2001).

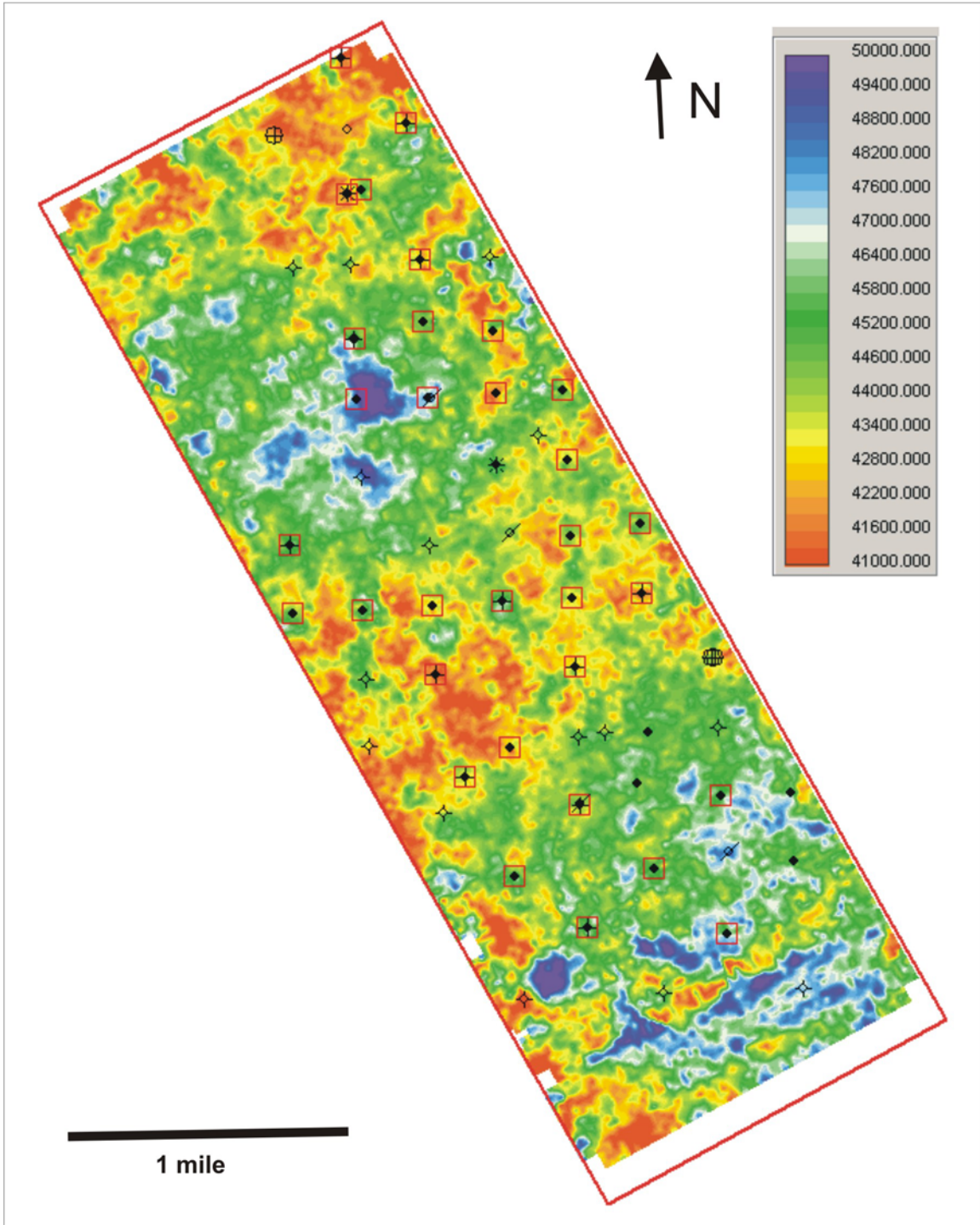


Figure 2.2.24. Average acoustic impedance for the Spergen interval from a model based inversion volume. Purple corresponds to highest impedance and red corresponds to lowest impedance.

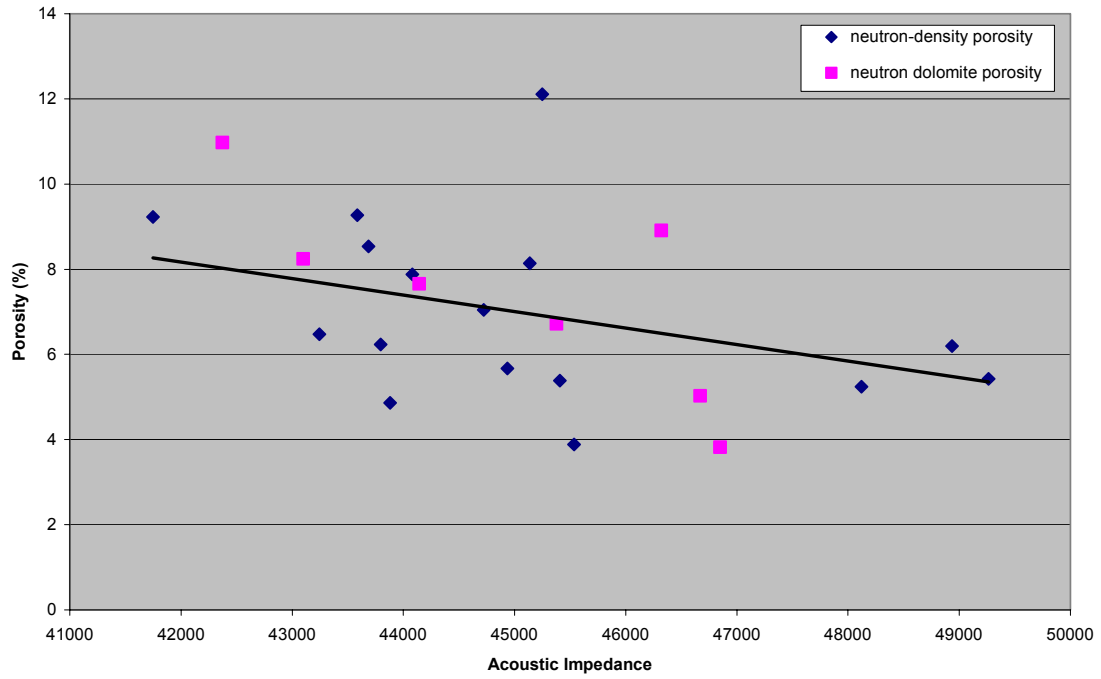


Figure 2.2.25. Crossplot of wireline log porosity versus acoustic impedance extracted from the model-based inversion volume. Blue symbols are average neutron-density porosity. Purple symbols are neutron porosity on a dolomite scale.

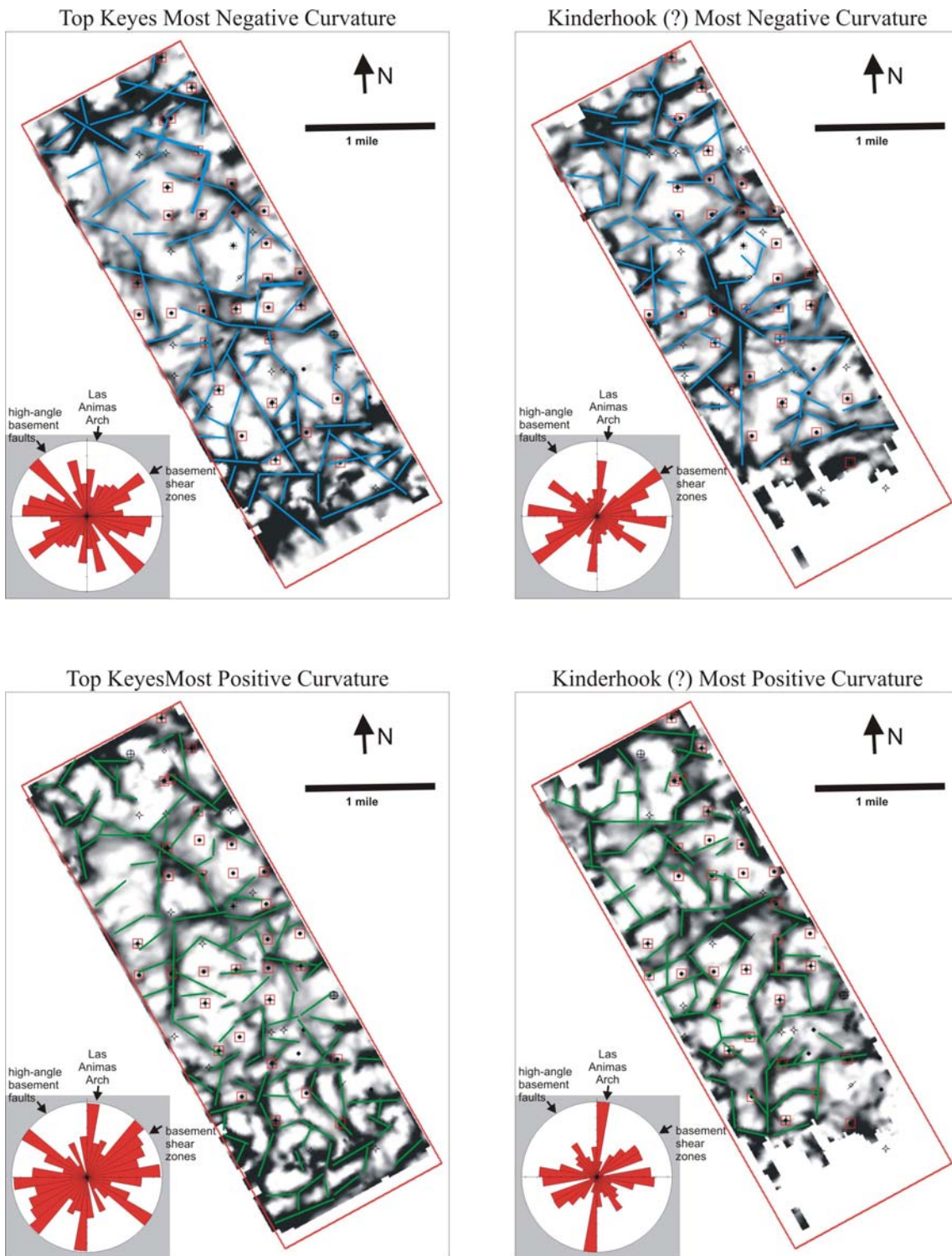


Figure 2.2.26. Most Positive and Most Negative curvature extractions along the Top Keys and Kinderhook horizons. Tighter curvature is shown in black and dark gray. Orientations of interpreted negative curvature (blue) and positive curvature (green) lineaments have been analyzed using length-azimuth rose diagrams (red).

Kansas

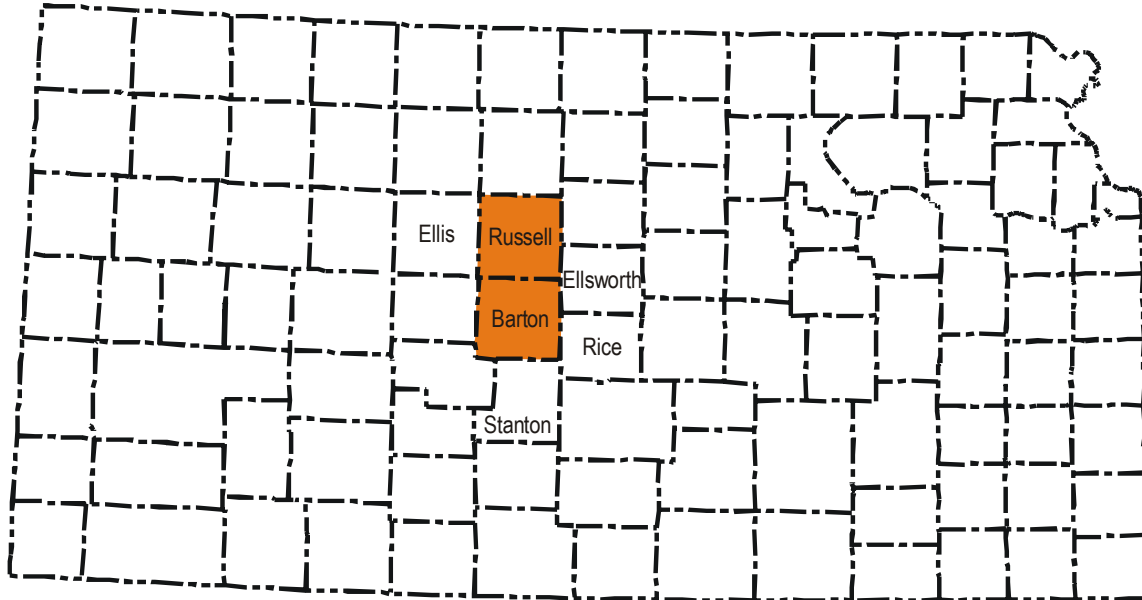


Figure 2.3.1 Map of Kansas showing location of regional Arbuckle study area covering Russell and Barton counties. Other counties mentioned in the report are labeled.

Era	System	Series	Stratigraphic Unit
Pennsylvanian	Virgilian		Wabunsee Group
			Shawnee Group
			Douglas Group
	Missourian		Lansing Group
			Kansas City Group
			Pleasanton Group
	Desmoinesian		Marmaton Group
			Cherokee Group
	Ordovician	Lower	
			Arbuckle Group
Cambrian	Upper		Reagan Sandstone
			Granite, Schist
Precambrian			

Hushpuckney Shale
Sniabar Ls.
Mound City Shale

Nuyaka Creek Shale
Nowata Shale
Altamont Ls.
Bandera Shale
Pawnee Ls.
Labette Shale
Fort Scott Ls.

Figure 2.3.2. Stratigraphic column for the Arbuckle study area in Russell County, Kansas, showing Pennsylvanian strata discussed in this report.

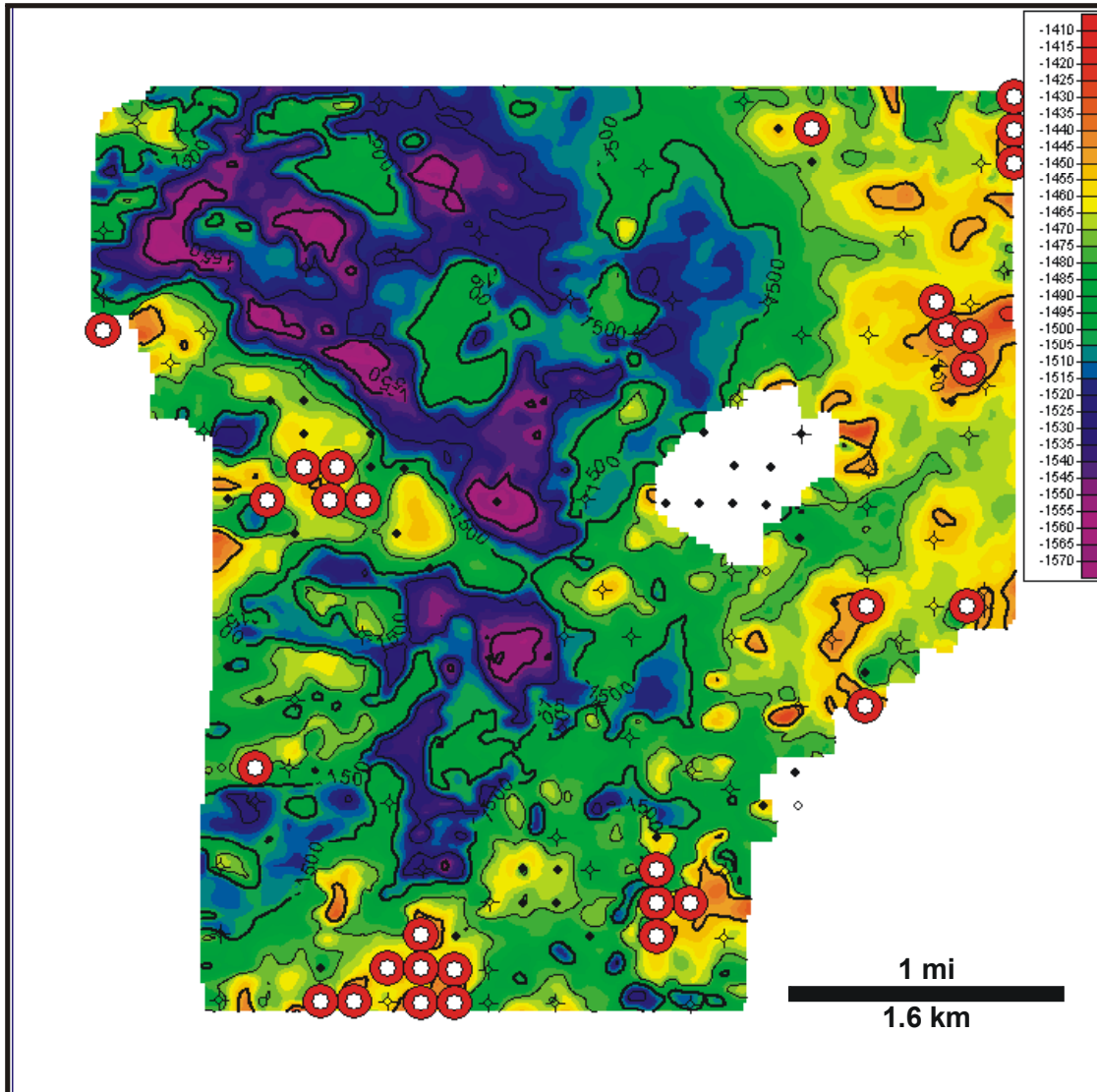


Figure 2.3.3. Arbuckle structure map depth-converted from 3-D seismic horizon time interpretation. Wells that penetrate the Arbuckle are displayed and those with Arbuckle production are highlighted in red.

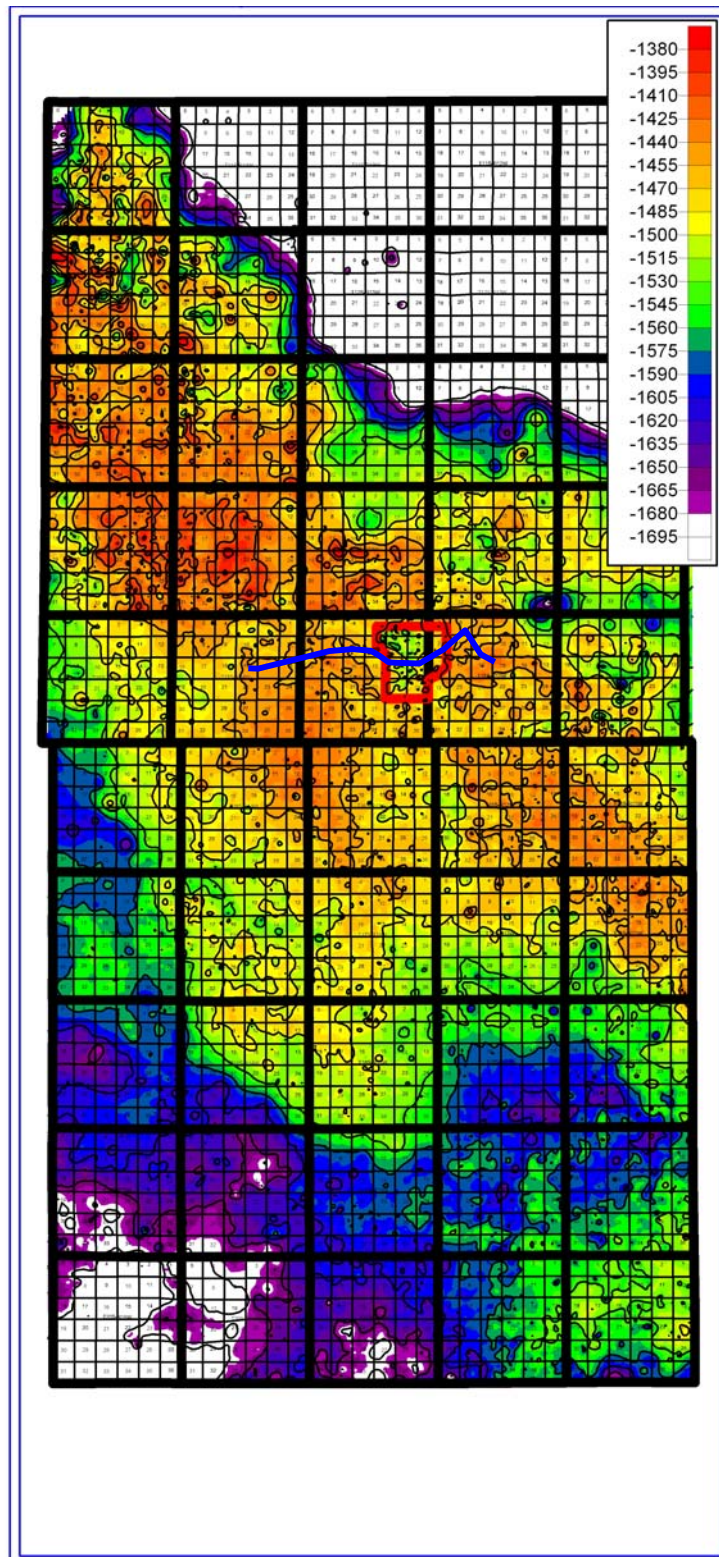


Figure 2.3.4. Arbuckle surface over the Central Kansas Uplift in the study area including Russell and Barton Counties. Red outline indicates area of 3-D seismic data. The location of cross section *A-A'* in Figure 2.3.8 is shown by the blue line.

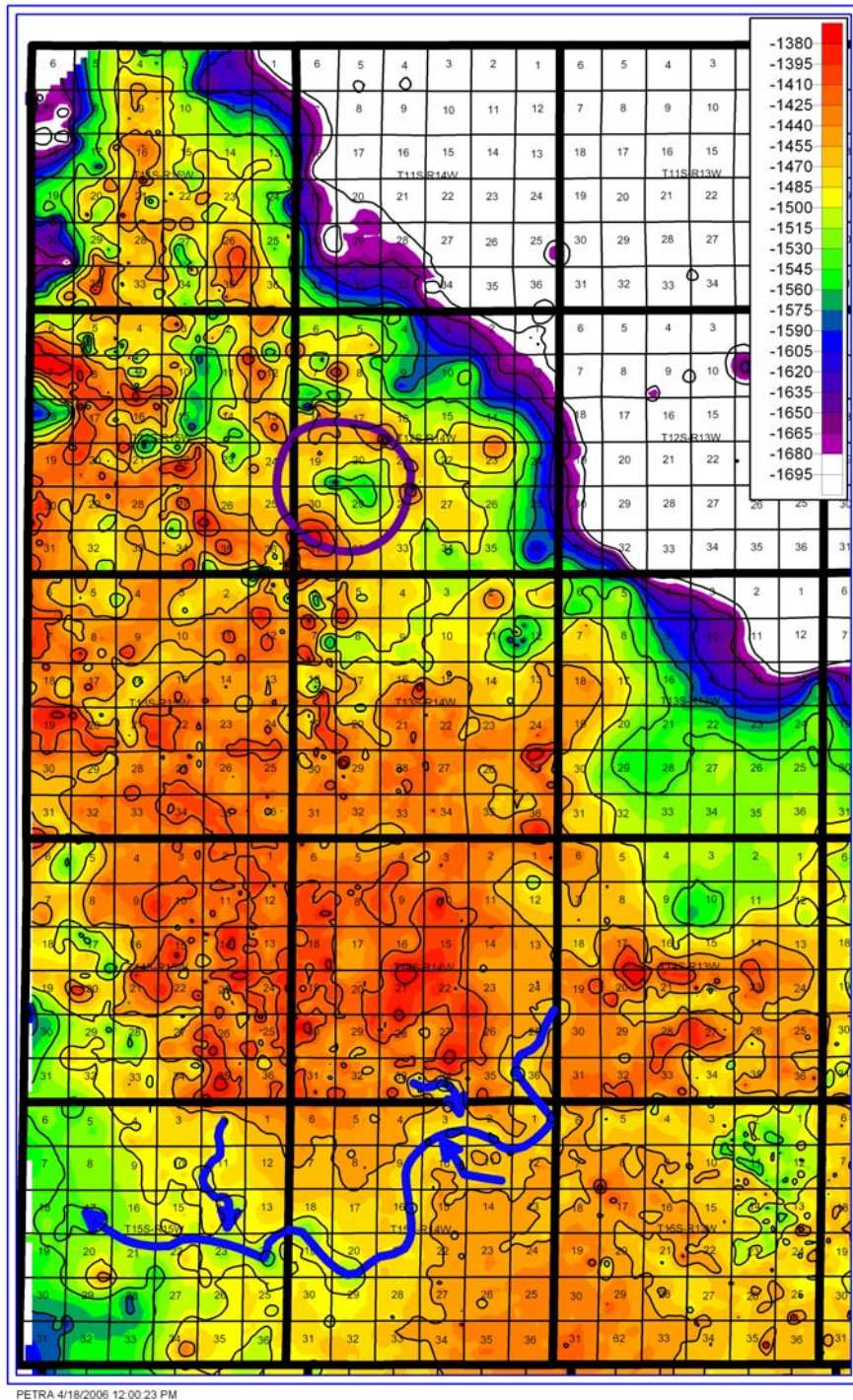


Figure 2.3.5. Detail of Arbuckle surface showing karst features. Blue line indicates groundwater sapping processes creating half-blind valleys. Purple line indicates polygonal karst.

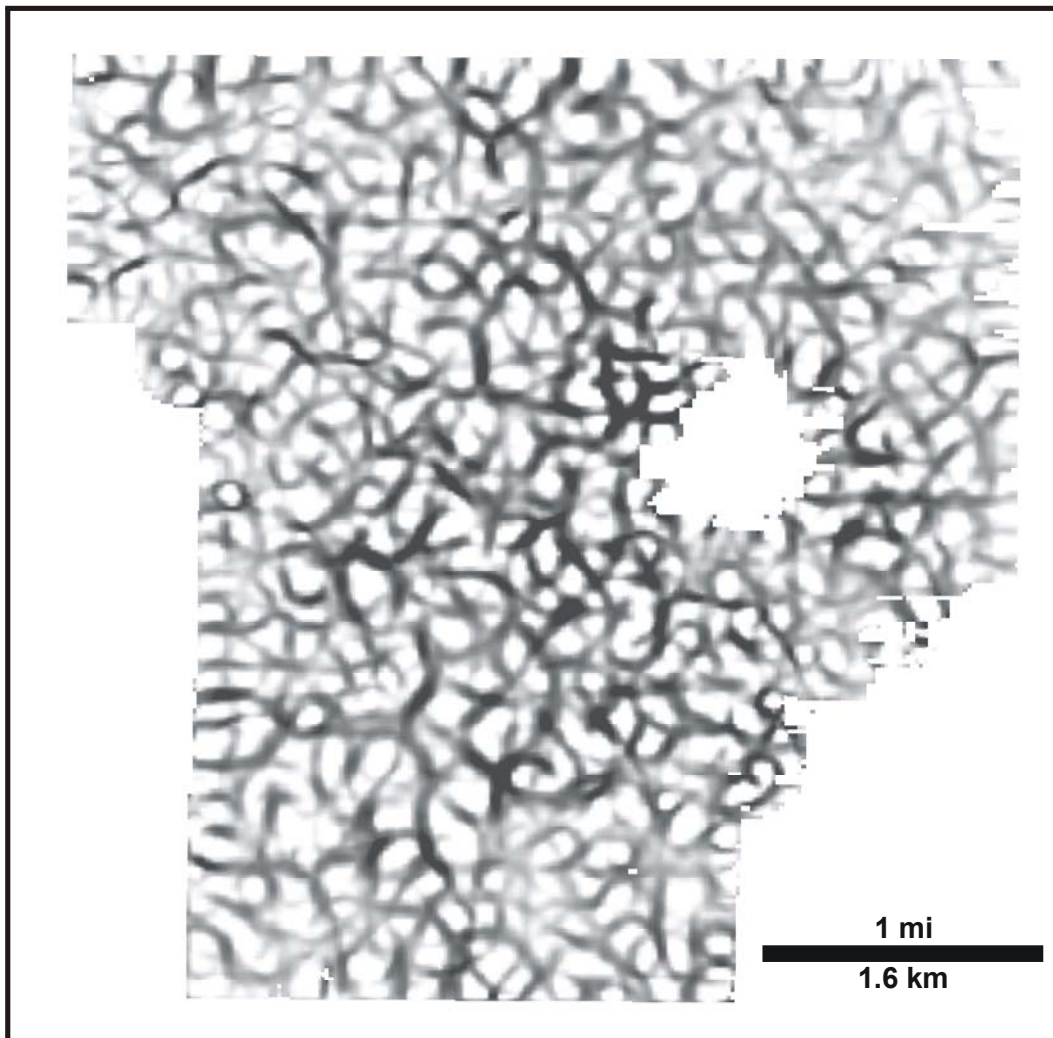


Figure 2.3.6. Volumetric Most Positive curvature extracted along the Arbuckle horizon from the Russell County, Kansas, 3-D seismic survey. This map shows a network of polygonal features reminiscent of polygonal or cockpit karst. Most Positive curvature is scaled so that dark areas indicate high curvature.

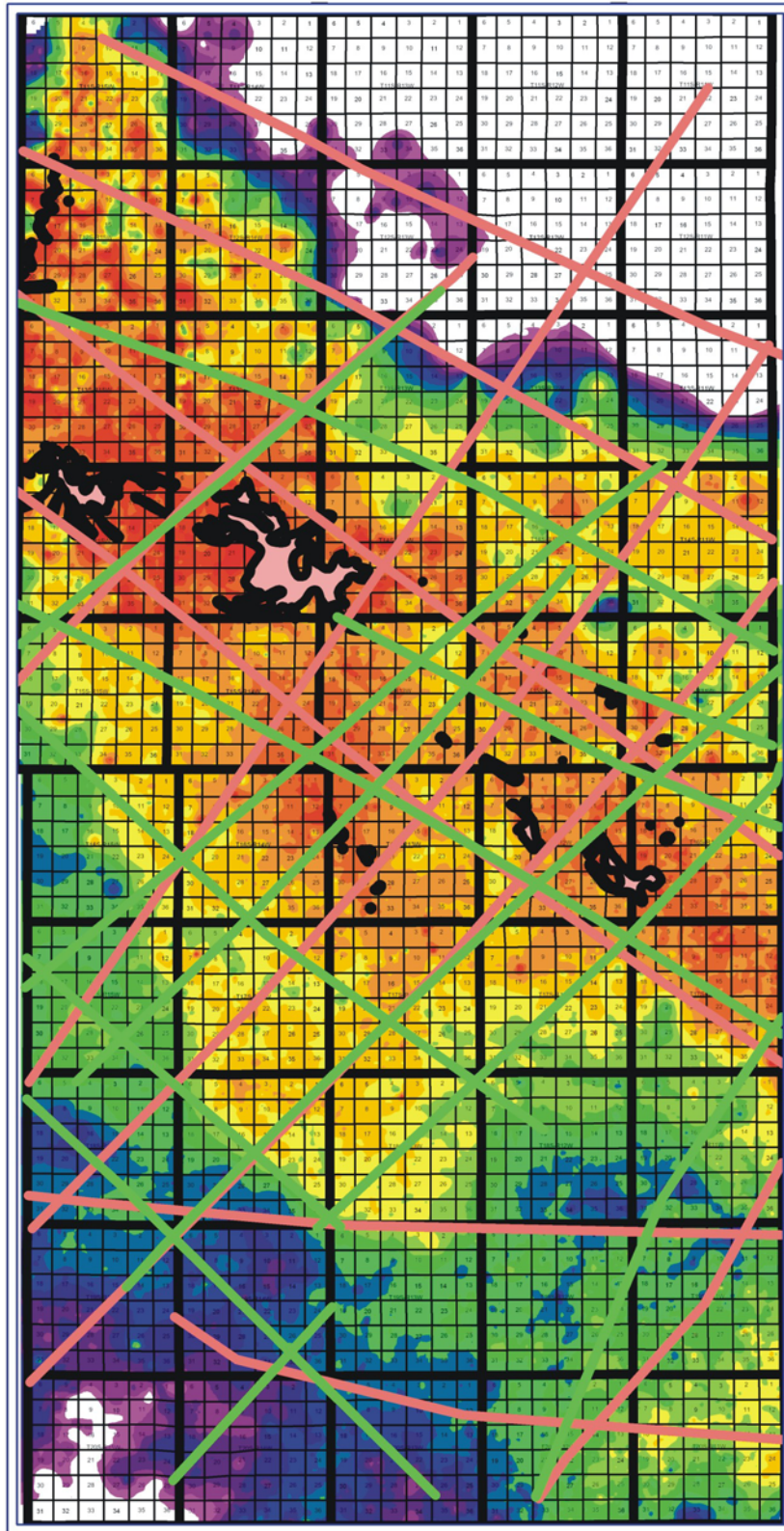


Figure 2.3.7. Arbuckle surface with magnetic (green) and gravity (pink) lineaments. Pink blobs are areas where Arbuckle strata are absent and Precambrian basement was exposed.

Arbuckle Project in Petra

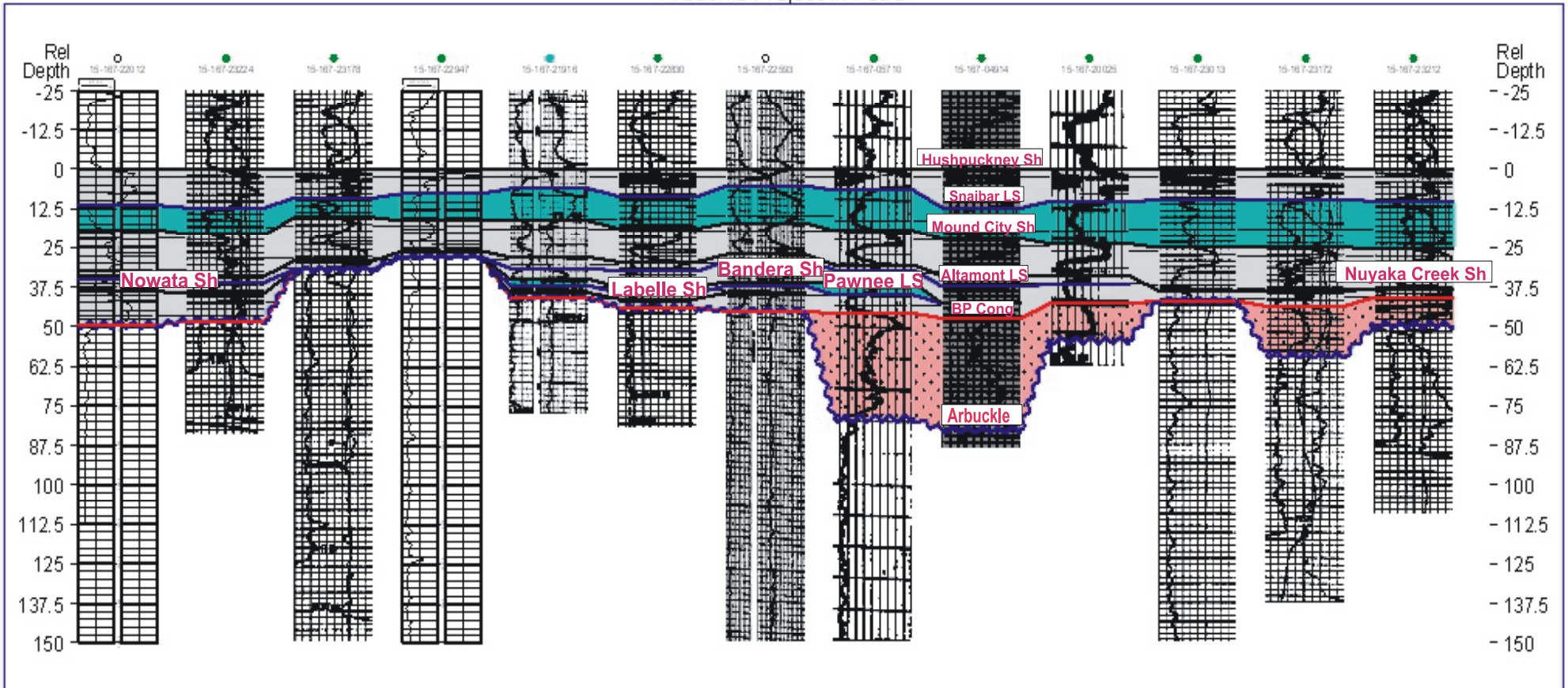


Figure 2.3.8. West to east cross section across Central Kansas Uplift showing onlapping of Pennsylvanian strata. Fourth track from left is topographically the highest Arbuckle strata. Datum is Hushpuckney Shale Member. The oldest formation overlying the crest of the Arbuckle is the Nuyaka Creek Shale Member. Blue fill is limestone, gray fill is shale, and pink fill is basal Pennsylvanian conglomerate.

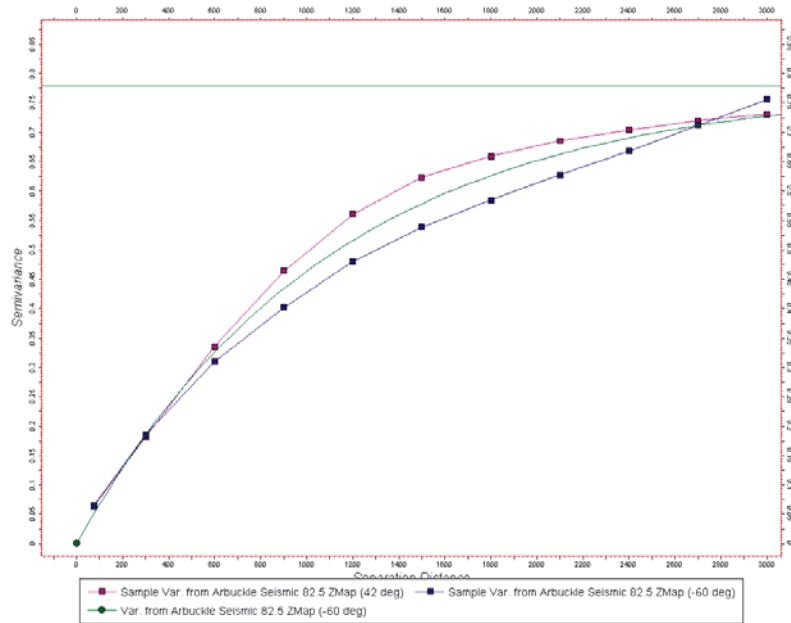


Figure 2.3.9. Variogram from seismic data (pink and purple lines) and model (green line).

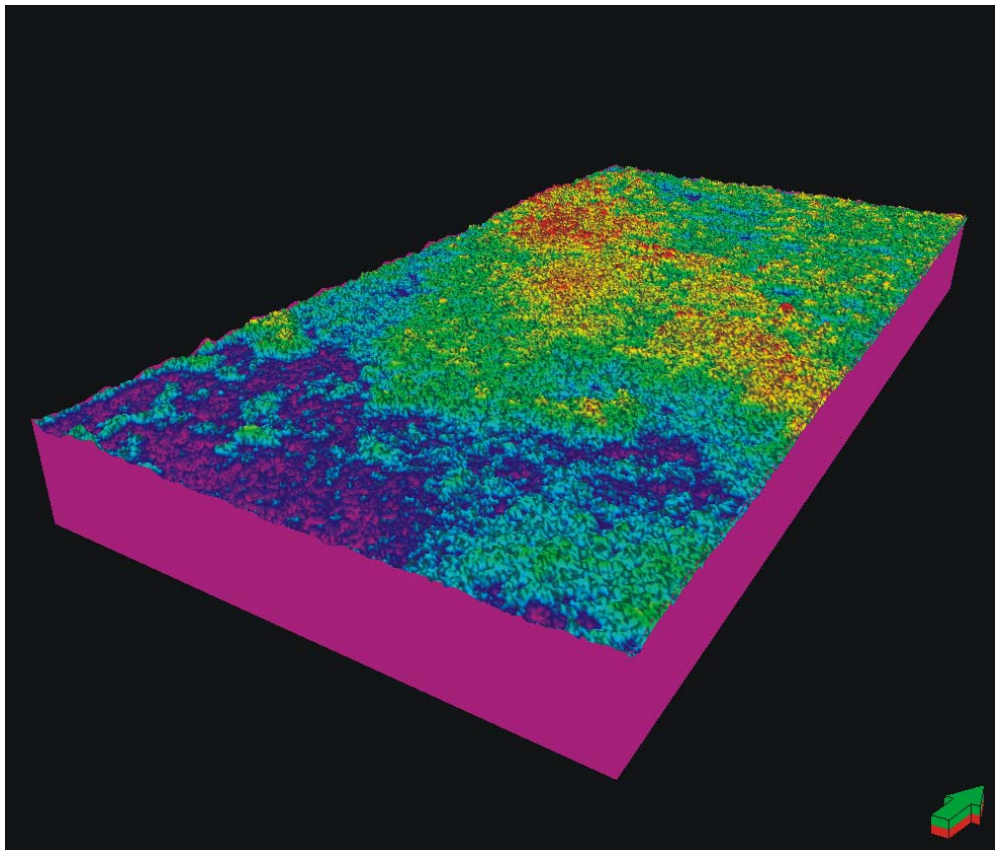


Figure 2.3.10. 3-D image of simulated roughened surface of the Arbuckle. Boundaries of the map are those of Russell and Barton Counties. Vertical exaggeration=20x.

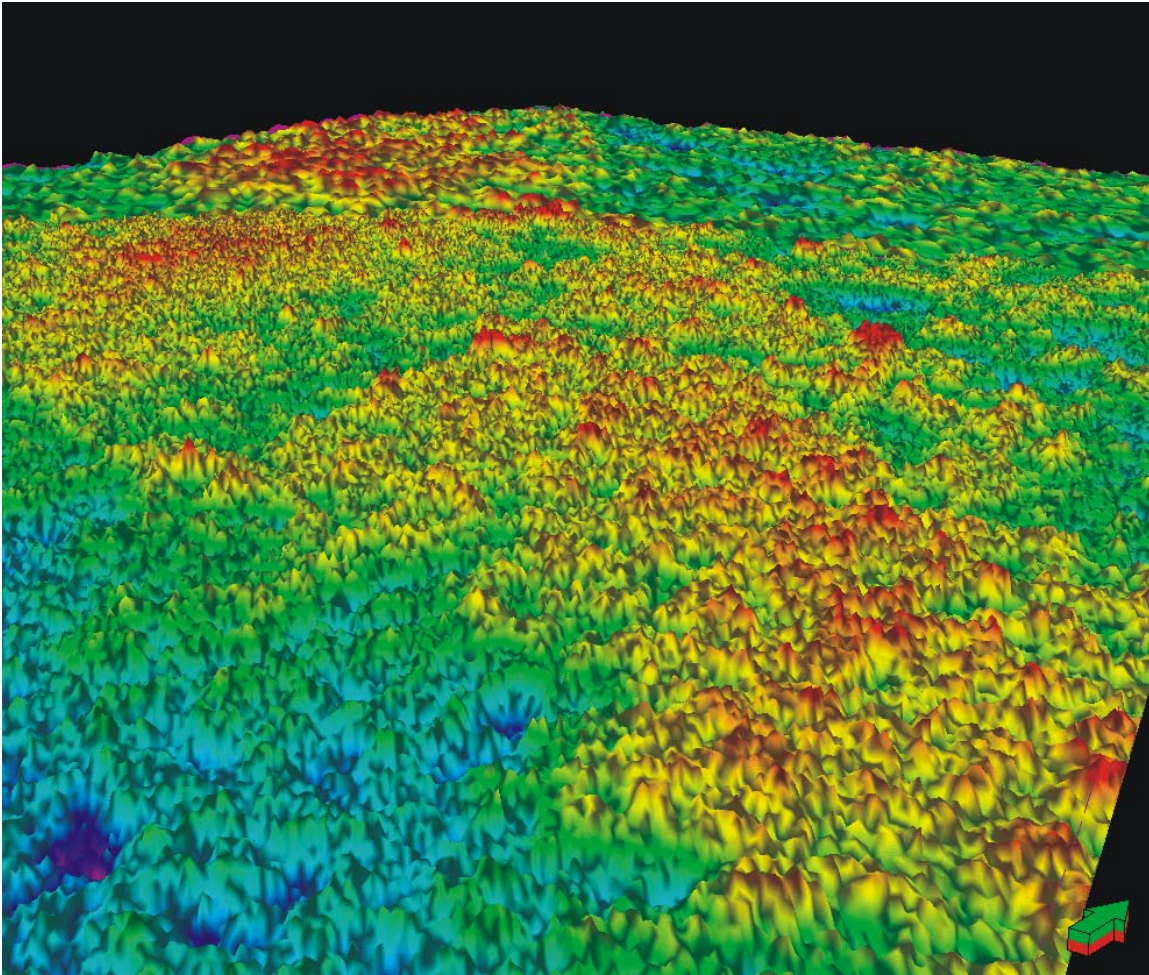


Figure 2.3.11. Close-up of roughened surface of Arbuckle looking along the crest of the Central Kansas Uplift. Vertical exaggeration=20x.

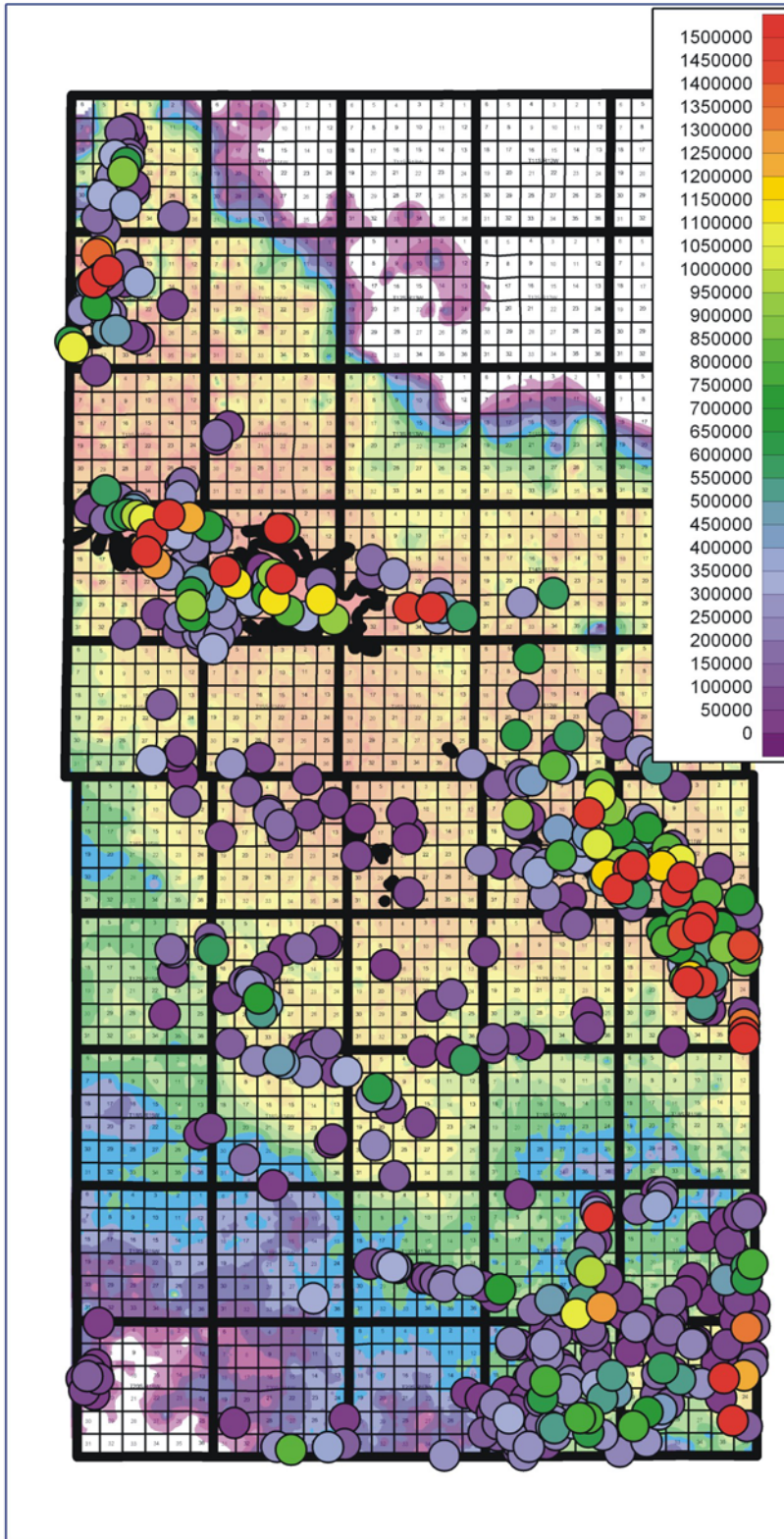


Figure 2.3.12. Arbuckle cumulative production data bubbles on washed-out Arbuckle structure background. Scale to the right begins at the bottom (purple) with 0 barrels of cumulative production, and ends at top (red) with 1,500,000 barrels of cumulative production.